Norwegian University
of Life Sciences

Master's Thesis 2019 30 ECTS
Faculty of Environmental Sciences and Natural Resource Management

Urban Wind Energy – The Effect of Obstacles and Buildings

Daniel Lunder Husøy
Renewable Energy

ABSTRACT

This master´s thesis is completed as a part of the master's degree in renewable energy at the Norwegian University of Life Science at Ås. As we can see in the later years, the interest for urban wind energy utilization is increasing and different challenges arise. The main objective of this thesis was to investigate how buildings affect the annual energy production on commercial-scale wind turbines in urban areas. The WindSim software was used to make wind field simulations and to construct simulation areas. To verify that WindSim is a sufficient software to use for such tasks, a validation test was made out of a wind tunnel experiment and the same experiment simulated in WindSim. The blocking-file function in WindSim was explored and used to build obstacles and buildings. The results show that WindSim is a sufficient software to use for such simulations and the experiment is well matched to the wind tunnel experiment studied. Furthermore, a case study at Borg Havn in Fredrikstad was carried out. Based on the wind tunnel verification that was done, a comparison between Borg Havn with and without buildings were done. The results of this study show a minimal effect from buildings on the annual energy production in urban areas.

SAMMENDRAG

Denne masteroppgaven er utført ved Norges miljø- og biovitenskapelige universitet på Ås som en del av mastergraden i fornybar energi. I de senere år har man sett en økende interesse i å produsere energien der man trenger den, ofte i urban områder, noe som fører med seg ulike utfordringer. Hovedmålet med oppgaven var å undersøke hvordan bygninger påvirker den årlige energiproduksjonen på små-skala vindkraft i urbane områder. Programmet WindSim ble brukt for å gjøre vindfeltberegninger. For å verifisere at WindSim er et tilstrekkelig program å bruke for slike oppgaver ble det gjort en valideringstest mellom en vindtunneltest og samme test simulert i WindSim. Samtidig med dette ble «blocking-file» funksjonen i WindSim utforsket. Resultatene viser at WindSim er et tilstrekkelig program å bruke til slike simuleringer og eksperimentet samsvarer godt med vindtunnel-testene som ble studert. Videre ble en case studie på Borg Havn i Fredrikstad utført. Med bakgrunn i valideringen som ble gjort, ble det videre foretatt en studie med hensyn på bygninger i nærheten av to lokasjoner. Resultatene fra studien viser en minimal effekt på den årlige energi produksjonen fra bygningene, sammenlignet med scenarioet uten bygninger. Ut ifra resultatene kan det konkluderes med at WindSim er et egnet program og bygningene ikke har en så stor effekt på den årlige energiproduksjonen.

ACKNOWLEDGMENTS

Firstly, I want to sincerely thank Arne Gravdahl for extraordinary mentoring on this thesis. Thank you for the assistance and follow up on different problems that have occurred throughout this journey. I also want to thank the WindSim team for holding a course in WindSim, as well as opening their office space and helping out with different challenges. Thank you to Borg Havn and Smart Innovation Norway, especially Marianne Kahrs, for wanting to involve me in their exciting new project at Borg Havn. Lastly, I must thank my classmates at the Norwegian University of Life Science at Ås for two remarkable years at NMBU. Great company during hard exam periods and a lot of interesting conversations during coffee breaks.

Daniel Lunder Husøy

Norwegian University of Life Science, Ås
13.05.2019

TABLE OF CONTENTS

TABLE OF FIGURES

TABLES

1 INTRODUCTION

The utilization of wind power has existed for thousands of years. In the start, the wind energy was used to propel boats along the Nile river, and by the 11th century windmills were used in the Middle East extensively for food production as well as cutting wood (EIA, 2018). The early norther European windmills were used for any mechanical tasks such as water pumping, grinding grain, sawing wood and powering tools (Manwell et al., 2009). In the late 1960s a re-emergence of wind energy began as a consequence of increased awareness to the environmental consequences of industrial development (Manwell et al., 2009). The potential dangers of nuclear energy and fossil fuels became more public and led to an environmental movement which began to support cleaner sources of energy (Manwell et al., 2009). The Oil Crisis in the mid-1970 started a new effort to develop alternative sources of energy, such as wind energy (Manwell et al., 2009). In the early 1980s, thousands of wind turbines were installed in California, as a result of federal and state policies that encouraged the use of renewable energy sources (EIA, 2018). In the 1990s and 2000s U.S federal government established further tax and investment incentives for wind power projects due to a renewed concern for the environment (EIA, 2018).

The development of renewable energy sources has in the latest years increased severely due to higher interest and demand for green energy, and a broader political support. Wind farms are being built all over the world, both on-shore and off-shore. Today we also see a growing trend and an interest for the use of small-scale wind power facilities in urban areas. The development has been there for quite a few years but have mostly included small-scale roof mounted turbines. Now, we rather see an interest in larger commercial-scale turbines, established at a port or industrial area. This is based on the demand of local produced energy and as a result of incentives to make the industry utilizing more green energy. The reason for this is the highly evaporating demand for energy close to where you need it. Also, the advantage of taking a shortcut around the electrical grid to avoid loss due to e.g. the transmission lines. Thus, there are a lot of pros to establish local green energy production and the potential is to be seen as great.

The same trend that happened earlier is evolving in the present. Since the support for a greener community and an increase in political support and funding, the interest in utilizing the wind in urban areas has increased. This is due to the same factors which arose for larger wind farms in the late 20th century. As urban wind energy development is arising, new and different problems appear.

This master thesis will focus on the location of a wind turbine in an urban environment and mainly the effect of buildings on the wind flow around them. This may lead to a reduced power production for local utilization of green power. The research question is formulated as the following;

"How do buildings affect the annual energy production for a wind turbine in an urban environment?"

The main method to embrace this task is by using WindSim to simulate the flow patterns and post process the results. A study of existing scientific literature is done with the emphasis on finding experimental results to validate these simulations. The validating method is mainly focused on wind-tunnel tests. To complement this, a real-life case study at the port of Borg Havn in Fredrikstad, Norway, is going to be evaluated. They aim to develop a commercial-scale wind turbine located at their port for self-produced green energy.

As mentioned above, there is a sever interest in local green energy production, and urban wind comes as a possible solution to complement other energy resources. Therefore, further knowledge and research on the different aspects of urban wind exploitation is highly needed and this thesis will try to resolve the main issue, buildings.

2 THEORY

2.1 WIND

2.1.1 WIND POWER

The available wind power is calculated by using the mass flow of air. The mass flow of air is characterized as dm/dt (Manwell et al., 2009). By using a rotor disc with area, A, air density ρ and air velocity U, the mass flow rate can be determined by utilizing equation (2.1) (Manwell et al., 2009). The air density under standard conditions is set to 1.225 kg/m^2.

$$\frac{dm}{dt} = \rho AU \tag{2.1}$$

Further on, the kinetic energy per unit time of the flow can be expressed as:

$$P = \frac{1}{2}\frac{dm}{dt}U^2 = \frac{1}{2}\rho U^3 \tag{2.2}$$

This leads to the wind power per unit area, power/area, also expressed as power density:

$$\frac{P}{A} = \frac{1}{2}\rho U^3 \tag{2.3}$$

2.1.2 WIND PROFILE

A wind profile is used to describe the relationship between the vertical distribution of horizontal mean wind speed related to height above the ground, within the lower region of the planetary boundary layer (Emeis & Turk, 2007). To estimate the mean wind speed, u_z, at a height z in meters, equation (2.4) is used (Beller, 2009). Where u_* is the friction velocity, κ is the Von Kármán constant set to around 0.41, d is the zero-plane displacement and z_0 is the surface roughness (Manwell et al., 2009). The zero-plane displacement is the height in meters above the ground, where zero wind speed is achieved as a result of flow around obstacles such as buildings. Approximately 2/3 to 3/4 of the average height of the obstacle (Holmes, 2018).

$$u_z = \frac{u_*}{\kappa}\left[\ln\left(\frac{z-d}{z_0}\right)\right] \tag{2.4}$$

For a uniform wind profile, the vertical distribution is uniform, and the horizontal wind speed is therefore equally distributed to the top of the boundary layer. An example for a logarithmic and uniform wind profile is shown in Figure 2.1.

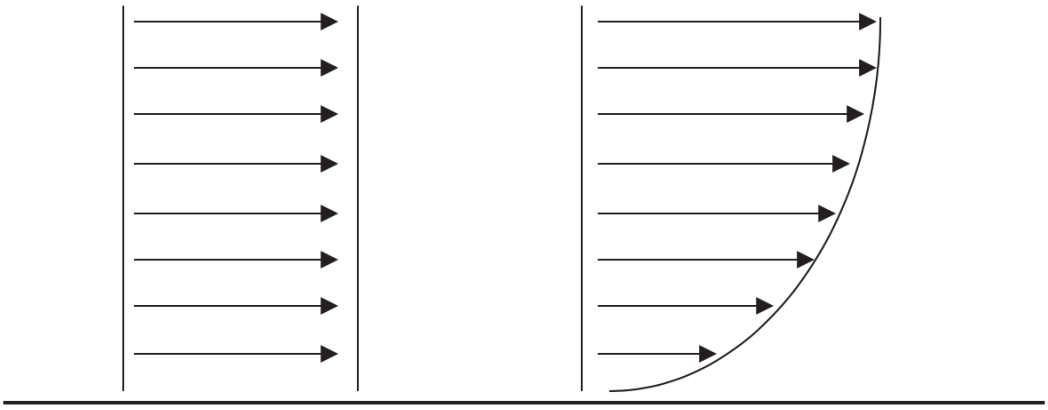

Figure 2.1: Uniform and logarithmic wind profile distribution

2.2 Atmospheric Boundary Layer

The atmospheric boundary layer (ABL), also called boundary layer or planetary boundary layer, is the lowest part of the atmosphere, which is the layer closest to the earth's surface (Manwell et al., 2009). On clear nights with low wind speeds it extends to about 100 m above ground, while on fine summer days up to 2 km (Troen & Petersen, 1989). At this level; velocity, temperature and relative humidity can rapidly change in space and time (Troen & Petersen, 1989). The surface friction directly affects the wind in the ABL, which leads to weaker wind speeds (Troen & Petersen, 1989). ABL is important regarding estimation of wind resources because of the variation of wind speed related to height above the surface, which influences the wind profile. Stability in the atmospheric boundary layer is an important characteristic to determine the wind speed gradients. These occur in the first few hundred meters above the ground (Manwell et al., 2009). There are three classifications of atmospheric stability; stable, neutrally stable or unstable (Manwell et al., 2009). In Figure 2.2 you can see the vertical structure of the atmosphere.

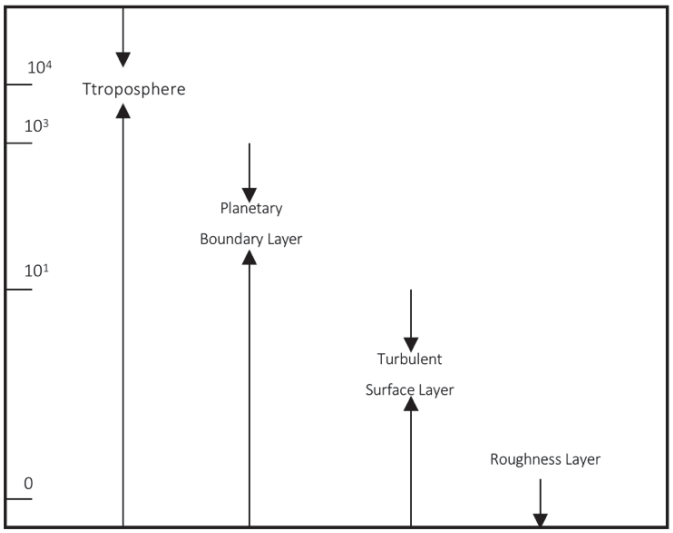

Figure 2.2: Different layers in the atmosphere in km, adopted from (Oke, 2002)

2.3 Computational Fluid Dynamics

2.3.1 Eddies

When a fluid is swirling, and reverse currents are created, the turbulent flow regime is called an eddy in fluid dynamics (Chiu & Chien, 2011). It is a circulation that develops when wind flows over e.g. buildings or mountains (Integrated Publishing, n.d.). On the lee side of an obstacle eddies are normally formed. The size of the obstacle and speed of the wind directly affects the size of an eddy, and may form horizontal or vertical circulations (Integrated Publishing, n.d.). In fluid mechanics an eddy is not a property of the fluid, but rather a violent swirling motion caused by the position and direction of turbulent flow (Schoch et al., 2008)

2.3.2 Vortex

Vortices is one of the most important aspect of turbulent flow (Majda & Bertozzi, 2002). A region in a fluid in which the flow revolves around an axis line, which may be straight or curved is a vortex (Kida, 2001). Vortex dynamics is the interaction of local swirls or eddies in the fluid (Majda & Bertozzi, 2002). To mathematically study vortices you analyze the rotation or curl of the velocity field, this is called vorticity (Majda & Bertozzi, 2002). A chaotic system with vortices is called turbulence.

2.3.3 ROUGHNESS

The roughness of a surface area is used in different numerical models to express the roughness of a surface. It is determined by the size and distribution of the roughness elements it contains (Troen & Petersen, 1989). This characteristically include for land surfaces vegetation, built-up areas and the soil surface (Troen & Petersen, 1989). The roughness length of the terrain is usually expressed as z_0, which is a parameter of a vertical wind profile that model the horizontal mean wind speed near the ground (Troen & Petersen, 1989). High above ground level, at around 1-kilometer height, the wind is hardly influenced by the surface of the earth, while in the lower layers of the atmosphere, wind speeds are affected by the friction against the surface of the earth (Danish Wind Industry Association, 2003). A large deviation indicates that the surface is rough, and if they are small, the surface is smooth (Danish Wind Industry Association, 2003). Forests and large cities obviously slow the wind down considerably, but on the other hand, you have concrete runways in airports that only slow the wind down a little (Danish Wind Industry Association, 2003). An even smoother surface is water and will have even less influence on the wind (Danish Wind Industry Association, 2003). A table of terrain classification is shown in Table 1. To calculate the roughness height, equation (2.4) can be used which is the logarithmic law (WindSim, 2019).

Table 1: Terrain classification (Wieringa, 1998)

Class	Roughness length (m)	Landscape features
Sea	0.0002	Open water, tidal flat
Smooth	0.005	Featureless land, ice
Open	0.03	Flat terrain with grass, airport runway
Roughly open	0.10	Cultivated area, low crops, obstacles separated by at least 20H
Rough	0.25	Open landscape, scattered shelter belts, obstacles separated by 15H
Very rough	0.5	Landscape with bushes, young dense forest separated by 10H
Closed	1.0	Open spaces comparable with H
Chaotic	>2.0	Irregular distribution of large elements, city center, large forest

2.3.4 REYNOLD AVERAGE NAVIER-STOKES

The Reynolds Average Navier-Stokes equations (RANS) are time averaged equations of motion for fluid flow (Alfonsi, 2009). The flow of a viscous incompressible fluid with constant properties is governed by Navier-Stokes which further leads to the RANS equation in (2.5) (Alfonsi, 2009)

$$\rho \hat{u}_j \frac{\partial \hat{u}_i}{\partial x_j} = \rho f_i + \frac{\partial}{\partial x_j}[-\rho \delta_{ij} + \mu \left(\frac{\partial \hat{u}_i}{\partial x_j} + \frac{\partial \hat{u}_j}{\partial x_i} \right) - \rho u'_i u'_j] \tag{2.5}$$

2.3.5 REYNOLDS NUMBER

The Reynolds number (Re) is a number used to distinguish between laminar and turbulent flows (Bravard & Petit, 2009). The Re is dimensionless and Re smaller than 500, viscous forces dominate and the flow is laminar (Bravard & Petit, 2009). For Re larger than 2000, turbulent forces are dominant which means the flow is fully turbulent (Bravard & Petit, 2009). The Re is defined as the relationship between inertial and viscous forces. To find the Re equation (2.6) is utilized (Bravard & Petit, 2009)

$$Re = \frac{U\delta}{\nu} \rightarrow \frac{Intertial\ force}{Viscous\ force} \tag{2.6}$$

Where these are the parameters;

- δ : Thickness of the boundary layer
- U: Free stream velocity
- v: Kinematic viscosity of the air

2.4 TURBULENCE

Turbulence is the change in air motions that is covered on the wind's average motion. It is caused by dissipation of the wind's kinetic energy into thermal energy by the creation and destruction of progressively smaller eddies (Manwell et al., 2009). Over a shorter time span the turbulence may be quite variable, but on time periods of an hour or more it may have relatively constant mean (Manwell et al., 2009).

2.4.1 TURBULENCE INTENSITY

The Turbulence Intensity (TI) represents the intensity of wind velocity fluctuation and is defined as the ratio of standard deviation of fluctuating wind velocity to the mean wind speed (Manwell et al., 2009). The standard deviation, set in sampled form, is given by equation (2.7) (Manwell et al., 2009). By utilizing equation (2.8) with σ_u, the TI can be found.

$$\sigma_u = \sqrt{\frac{1}{N_S - 1}\sum_{i=1}^{N_S}(u_i - U)^2} \tag{2.7}$$

$$TI = \frac{\sigma_u}{U} \tag{2.8}$$

The mean velocity, *U,* can be computed by utilizing equation (2.9) with the velocity components in x-, y- and z-direction.

$$U = \sqrt{U_x^2 + U_y + U_z^2} \tag{2.9}$$

2.4.2 K-ε TURBULENCE MODEL

The standard turbulence model *k-ε* is one approach to calculate the turbulence. It is a part of the eddy viscosity model and by an analytical equation, the eddy viscosity, v_t, can be calculated by utilizing equation (2.10) (WindSim, 2019).

$$v_t = C_\mu \frac{k^2}{\varepsilon} \tag{2.10}$$

$$\begin{aligned} &(\rho\, k), t \;+\; \left(\rho\, Ui\, k \;-\; \left\{\rho \frac{\nu t}{PRT(k)}\right\} k, i\right), i \;=\; \rho\,(Pk \;-\; \varepsilon) \\ &\frac{\partial(\rho k)}{\partial t} + \frac{\partial(\rho k u_i)}{\partial x_i} = \frac{\partial}{\partial x_j}\left[\frac{v_t}{\sigma_k}\frac{\partial k}{\partial x_j}\right] + 2v_t E_{ij} E_{ij} - \rho\varepsilon \end{aligned} \tag{2.11}$$

$$\begin{aligned} &(\rho\, \varepsilon), t \;+\; \left(\rho\, Ui\, \varepsilon \;-\; \left\{\rho \frac{\nu t}{PRT(\varepsilon)}\right\} \varepsilon, i\right), i \;=\; \left\{\rho \frac{\varepsilon}{k}\right\} (C1\, Pk \;-\; C2\, \varepsilon) \\ &\frac{\partial(\rho\epsilon)}{\partial t} + \frac{\partial(\rho\varepsilon u_i)}{\partial x_i} = \frac{\partial}{\partial x_j}\left[\frac{v_t}{\sigma_\varepsilon}\frac{\partial \epsilon}{\partial x_j}\right] + C_{1\varepsilon}\frac{\varepsilon}{k}\, 2v_t E_{ij} E_{ij} - C_{2\varepsilon}\rho\frac{\varepsilon^2}{k} \end{aligned} \tag{2.12}$$

Equation (2.11) and (2.12) are used to find *k* and *ε* respectively. *k* is the turbulent kinetic energy and *ε* is the dissipation. E_{ij} represents the rate of deformation while u_i is the velocity constant in corresponding direction. The following constants has normally default values equal to the (Versteeg and Malalasekera (2007) as cited on Wikipedia contributors (2019))

- $C_{1\varepsilon} = 1.44$,
- $C_{2\varepsilon} = 1.92$
- $C_\mu = 0.09$
- $\sigma_\varepsilon = 1.30$
- $\sigma_k = 1.00$.

2.5 Flow Around Obstacles and Buildings

2.5.1 Wind climate

Around an obstacle the wind flow separates in different directions depending on the width, depth and height of the obstacle (Meroney, 1985). A common approach to consider the wind flow behavior around an obstacle is by looking at them as rectangular blocks and study the flow in two- or three-dimensions. For a two-dimensional flow around a simple geometric block this is shown in Figure 2.3. It develops a horseshoe vortex at the windward side of the obstacle. Also, the flow reattaches at the top. Another case could be that the flow does not reattach at the top (Meroney, 1985). You can also see that eddies are developed on the lee side, with smaller and larger whirls.

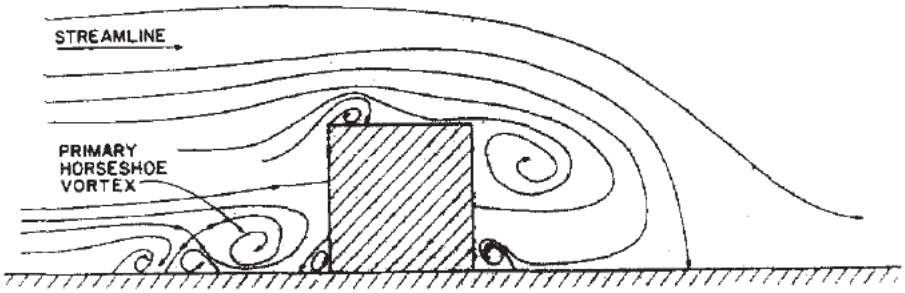

Figure 2.3: Flow around a 2D obstacle (Meroney, 1985)

Shown in Figure 2.4, the flow in two-dimension leads to a momentum wake and results in a free shear layer that separates from the top edge of the obstacle and reattaches downwind (Manwell et al., 2009). This forms a boundary between an inner recirculating eddy and outer flow region (Manwell et al., 2009).

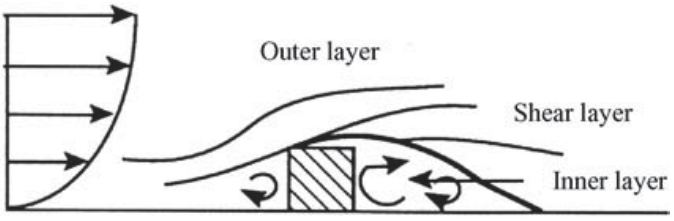

Figure 2.4: Momentum wake - 2D (Manwell et al., 2009)

Due to a shielding effect that will vary with the height above the site surface, the result of this will typically produce a distorted wind speed profile which is shown in Figure 2.5 (Nieuwpoort et al., 2010). The boundary of the internal layer that will develop behind the obstacle is also indicated in the figure. Here a wind speed, less than the wind speed which would occur in the undisturbed flow, is present. On the other hand, above the internal boundary the undisturbed wind speed profile is valid (Nieuwpoort et al., 2010). In Figure 2.5 it is assumed that the incoming air flow is perpendicular to the front side of the obstacle.

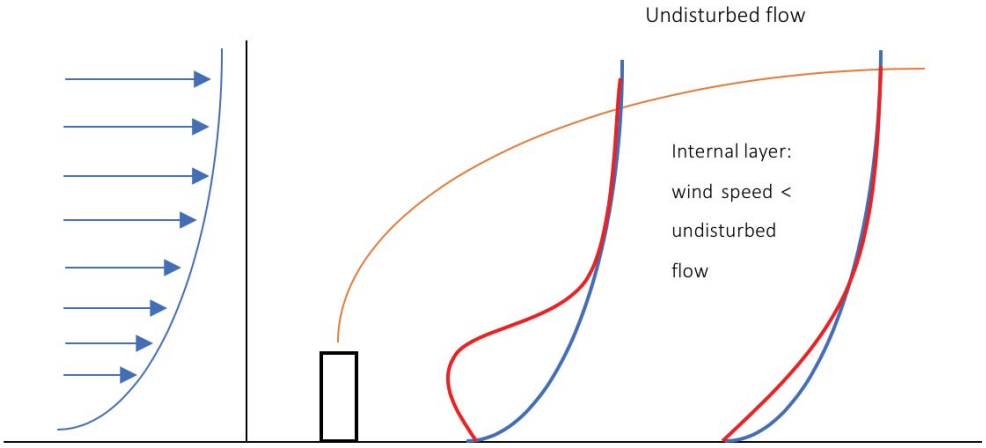

Figure 2.5: Air flow pattern depending on distance behind an 2D-obstacle, adopted from (Nieuwpoort et al., 2010)

For the mathematical wind flow modeling behind the obstacle, it is favorable that a symmetrical air flow can be adopted, which is not the case when the wind approaches the obstacle from a skew direction. This rather result in the creation of conical whirls on the top and sides of the obstacle, which again leads to an asymmetrical flow pattern (Nieuwpoort et al., 2010). At a large distance behind the obstacle, conical eddies, which are transported with the upward air flow, can be active (Nieuwpoort et al., 2010). In the case of an oblique air flow the wake area is smaller than for a perpendicular flow (Nieuwpoort et al., 2010).

Another way of describing the air flow around an obstacle is by looking at it at in a three-dimensional view. The schematic airflow around a building in three dimensions is shown in Figure 2.6. A more detailed sketch is shown in Figure 2.6 to the right.

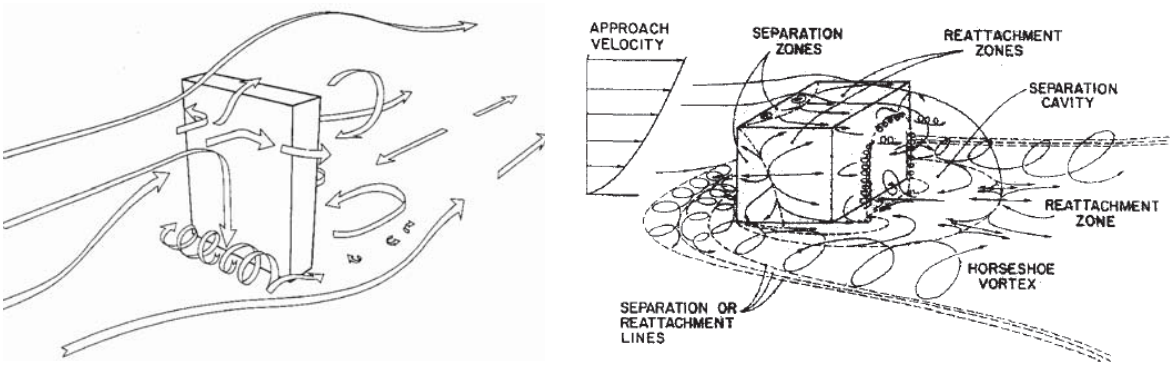

Figure 2.6: Airflow around a building in 3D (Meroney, 1985; Nieuwpoort et al., 2010)

As the wind approaches and hits the building the wind separates in different directions, both on the windward at the separation zones and leeward side, as well as on the obstacle sides. From the above figure you can also perceive different reattachment zones and lines. The wind gradually diverges until the stagnation point at three-quarter of the building height, and this result in the different up-and downward flows (Nieuwpoort et al., 2010). Below the stagnation point the air flow goes downwards and outwards and reaches the windward corners. When the air accelerates as it passes the corners and then generates two jets of air that extends for a substantial distance downwind. This is called the corner effect and can generate wind shear like phenomena (Nieuwpoort et al., 2010). Higher wind speeds around the corners can occur as a result of a longer and slimmer obstacle (Nieuwpoort et al., 2010). On the leeward side of the obstacle you also have separation zones which is generated. There is also a large amount of horseshoe vortices on this side.

2.5.2 Wake and turbulence

The wind shade and wake area are behind the obstacle. In this wake area, a relative slow wind speed is present. As a result of the transformation of high energy available in the airflow to gust and turbulence, when the airflow is slowed down significantly. The wake area is characterized by high turbulence levels that can be spotted at a relatively long distance behind the obstacle. In the same area a change in wind direction up to 180° may occur. Behind the obstacle the wake can extend to 4H or up to 5H times the obstacle, with height H. (Meroney, 1985). However, after the wake the original undisturbed speed profile is not directly resorted. From wind tunnel test the result shows that the disturbance may range to more than 15-20 times the obstacle height (Nieuwpoort et al., 2010). Whirls will develop starting from the corners of the obstacle as a result of the corner speeds and wake, because of the connection between the wake and corner streams. From the larger distances behind the obstacle, where speeds gradually decrease, the pressure slowly increases, and the air supply for the whirls is produced (Nieuwpoort et al., 2010). This leads to a flow that evolve in an opposite direction towards the obstacle. A formation of two large stationary whirls occur around a vertical axis in the wake area as an effect of the mentioned developed flow (Nieuwpoort et al., 2010). For a significant distance downwind from the obstacle a site will be shielded from the wind because of the wake.

2.5.3 Buildings

Obstacles such as buildings, cranes etc. are defined as man-made obstacles. These obstacles interfere with the flow of wind as a result of their width, height and depth, as well as the distance behind the building. Hence, this section transfers the knowledge about obstacles to buildings, which is the same in most cases but dissimilar when it comes to more complex shapes and structures.

The first factor to look at is maybe the most important factor, the height. The basic air flow patterns around a higher obstacle is not substantially changed, although the effect of a higher obstacle increases the air flow around the obstacle significantly (Nieuwpoort et al., 2010). As a result of increased corner streams the effect of the height also has a significant effect on the wake area (Nieuwpoort et al., 2010). The higher the obstacle, the larger the reverse flow area will be (Nieuwpoort et al., 2010).

Another important factor is also the width of the building obstacle. Wegley et al. (1980) established that only wide buildings with aspect ratio, width to height, of 3 or more produce a 10% or higher power loss at 20H with regards to power production from a wind turbine. With a constant height and depth, the increase in width will have a great effect on the magnitude of the wake area. For this scenario there appears no limit value (Nieuwpoort et al., 2010). Therefore, an increase in width will automatically lead to a larger wake area (Nieuwpoort et al., 2010).

Next is the depth, which may in many situations have a significant impact. A larger depth in relation to width and height a smaller wake area will develop as an effect of more than two times the height of the obstacle (Nieuwpoort et al., 2010). Thus, a thin obstacle creates larger whirls and more reverse airflow in the wake area (Nieuwpoort et al., 2010).

The third most important factor for the flow about buildings is the shape. The resulting wake characteristics and airflow patterns is highly affected by this (Nieuwpoort et al., 2010). When the obstacle deviates from the basic cube structure the wake characteristics can become progressively worse (Nieuwpoort et al., 2010). As an effect of increased top inclination, a larger wake area occurs (Nieuwpoort et al., 2010). Also, the top and top edges shape affects the likelihood of creating strong conical eddies (Nieuwpoort et al., 2010). The smoother and rounded forms are more fortunate to prevent these mentioned whirls.

The approaching air flow also needs to be mentioned since it also has a major effect on the flow around a building. A skew flow directed toward the obstacle may lead to the creation of strong conical rotating whirls (Nieuwpoort et al., 2010). Behind the obstacle, these whirls can be transported a great distance, and this may result in very complex and asymmetrical flow patterns (Nieuwpoort et al., 2010). In relation to the wake area an oblique air flow leads to a smaller wake area (Nieuwpoort et al., 2010). By looking at the above-mentioned factors, both the aspect ratio, direction and distance all have huge impact on the air flow around a building.

Also, a recirculation area is the zone directly behind the building with strong vortices and whirls (Nieuwpoort et al., 2010). This may extend quite a distance depending on height and depth. Behind this region there is a longer wake region where the flow velocity gradually recovers to its upwind value (Nieuwpoort et al., 2010). In this zone negative or reduced wind speeds will occur as the wind recirculates towards the building or building (Nieuwpoort et al., 2010). Shown in Figure 2.7, Wegley et al. (1980) recommends a distance from an obstacle of 20H in downwind and 2H in upwind direction, as well as 2H above ground.

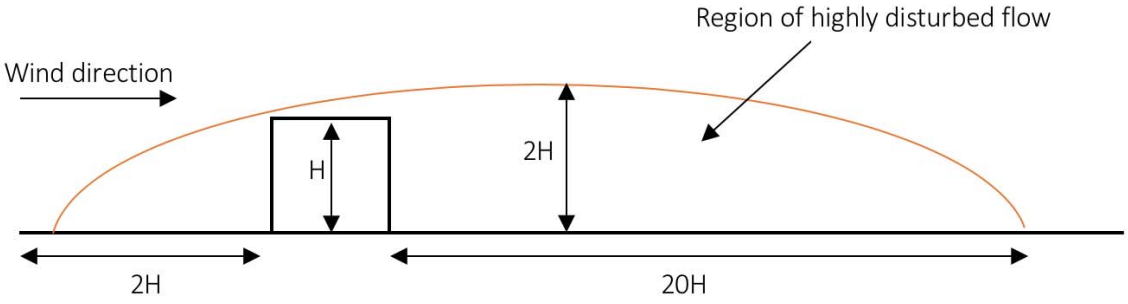

Figure 2.7: Zone of disturbed flow and recommended distance from an obstacle, adopted from (Wegley et al., 1980)

The estimates shown in Figure 2.8 apply at a level of one building height above ground level. The reduction gets smaller and smaller, and at 15H there is a significant reduction, and behind this it reattaches around 20H.

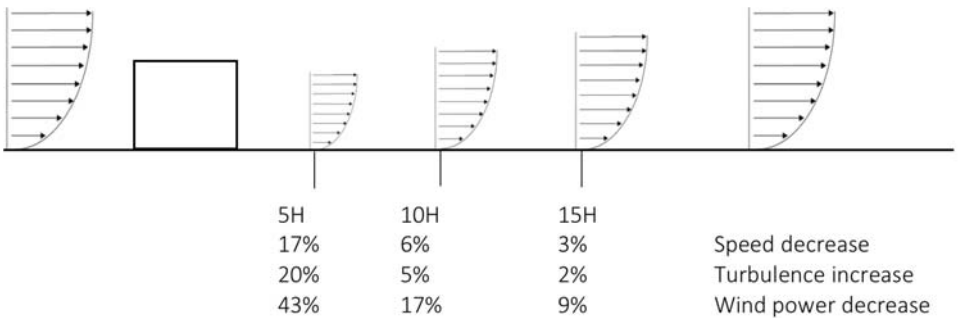

Figure 2.8: Speed, turbulence and wind power reduction downstream of a building, adopted from(Wegley et al., 1980 as cited in (Manwell et al., 2009))

2.5.1 Validation

Caniot et al. (2017) conducted a validation of a CFD tool called UrbaWind dedicated to wind assessment in urban area and also looked at applications of this. UrbaWind is based on the Navier-Stokes equations with a one-equation turbulence model (Caniot et al., 2017). Boundary conditions are automatically generated. In the Ekman layer the wind speed profile is a logarithmic function of geostrophic windspeed, windspeeds at the upper limit of the surface layer and above the ABL the wind speed is constant and equal to the geostrophic windspeed (Caniot et al., 2017). The geostrophic windspeed is based on a function of ABL height and the reference windspeed at 10m height in open land, roughness of 5 cm, defined at 10 m/s (Caniot et al., 2017).

A validation case of a wind tunnel experiment with group of blocks were utilized. The site was built up of 8 blocks of 20m of edge and an empty space in the center. A set up of the wind coming from the west and the result points located around the central empty space at two meters height the computations were done. UrbaWind was used to deduct speed-up factors and compared with the speed-up factors obtained by the experimental measures. The results of the simulation in UrbaWind and the comparison with the wind tunnel is shown in Figure 2.9 respectively. An error on the speed-up factor for the mean windspeed at 5.8% were discovered. The main errors come from low wind points or in an area of large gradients, close to the corners in particular (Caniot et al., 2017). The figure on the left shows a reduced speed-up factor behind the buildings in the wake, as well as a small reduction in front of the obstacle. Also, the figure shows that there exists no reattachment from the first row to the third row in between them.

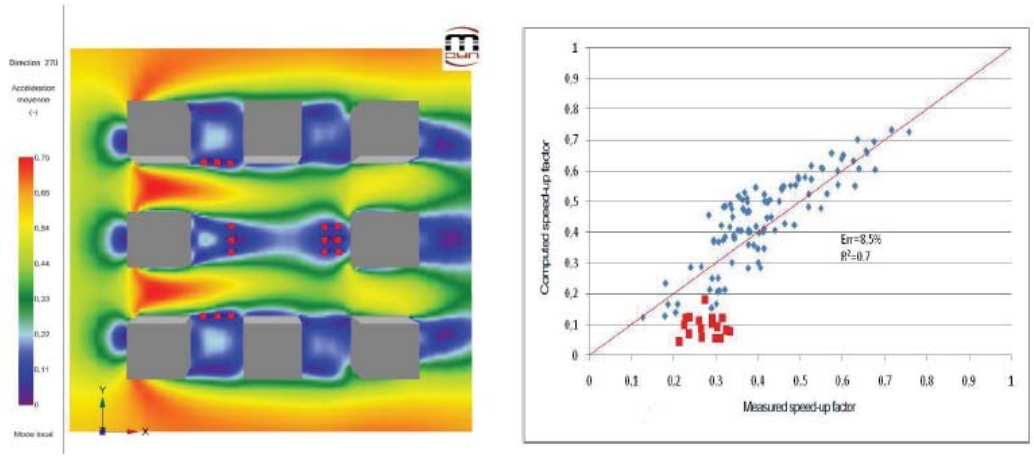

Figure 2.9: Wind flow around the lock, wind from left to right, and computed vs measured normalized wind speeds(Caniot et al., 2017)

Luo et al. (2012) studied models of cuboid obstacles to understand the dynamics of formation of shadow dunes behind obstacles. The approach was using scaled models in a wind tunnel, and the simulation were approximately independent of the Reynolds number. They further investigated the effect of different incidence angles and shape ratios. In Figure 2.10 you can see the horizontal and vertical cut planes from their study at a 90° incidence angle. They found that the flow separated both horizontally and vertically. This created reverse-flow cells downwind of the obstacle Luo et al. (2012). The flow patterns were similar regarding the different shape ratios; hence the incidence angle had a greater effect Luo et al. (2012). The wind velocity also had a relatively small effect on the flow patterns Luo et al. (2012). A separation both above and beside the obstacle, creating a reversed flow which generated a negative-velocity bubble. The blue area indicates the reversed flow. You can also see that the wake area extends about 4H behind the obstacle.

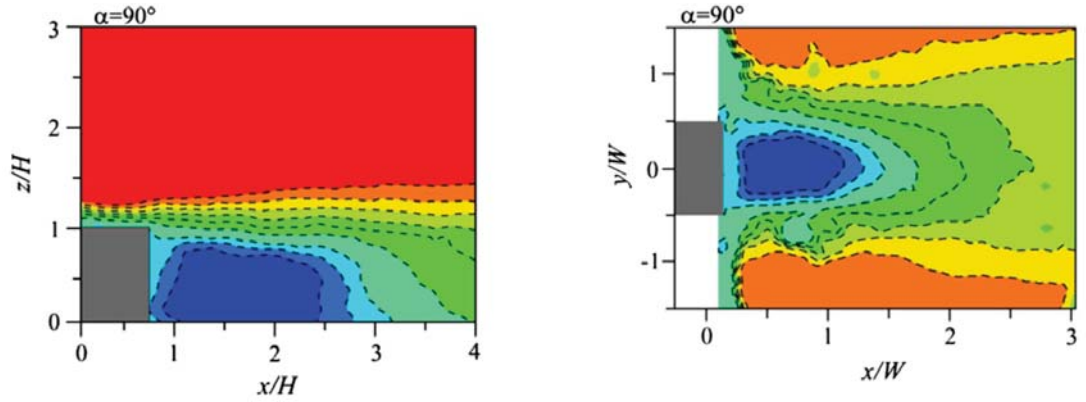

Figure 2.10: Cut planes with an incidence angle of 90° both vertical and horizontal respectively

Ntinas et al. (2014) did a study which aimed to predict the turbulent airflow around obstacles with arched and pitched roof geometry under wind tunnel conditions. They used a numerical model with a direct solution of a transient Navier-Stokes equation. To verify their study, an experiment was conducted inside a wind tunnel. Here they measured the air velocity and turbulent kinetic energy profiles around two small-scale obstacles with the mentioned roof geometry. Ntinas et al. (2014) concluded that the wind tunnel tests presented good agreement with the numerical simulations with respect to the airflow patterns. The effect of the different roof geometries was the instantaneous and time-mean averaged parameters on the flow. Ntinas et al. (2014) found that the results from the numerical solution indicated a fluctuating characteristic mainly downstream of the obstacles. In regards of streamlines and velocity components intense variations were shown for both arched-type and pitched-type, starting from the upstream corner of the roof and the top of the roof respectively (Ntinas et al., 2014). They

saw obvious effects on the downstream side of the obstacle, but no significant effect on the upstream side.

One of the most used and cited wind tunnel test in the reviewed literature is the test conducted by Castro and Robins (1977). They looked at the flow around a surface-mounted cube in a both a uniform and turbulent stream, also called a uniform and logarithmic wind profile. The wind tunnel setup was divided in two different models to look at the different cases. Case A was set as the uniform profile, while Case B was the logarithmic profile. Case A was utilized in a wind tunnel with dimensions 0.27x0.90 m, and Case B was in a 2.7x9.1m wind tunnel. The boundary layer was set to be 2m thick. The cube was positioned a distance of 3.5 times the boundary layer height downstream. A series of cubes for Case B was used, ranging from 20-80 mm. They also utilized the tests for a 45° attacking angle of the flow. Measurements were done around the cube and on the wake centerline. Ranging from -0.5H to 8.5H at different heights 0.3 to 1.0.

The results show that the reattachment occurs even for cube heights larger than the boundary-layer height. Although they comment that in their case the reattachment is probably alternating. Castro and Robins (1977) conclude that by comparing previous work, the velocity deficits in the wake is a strong function of the upstream turbulent intensities. Although their work show that the wake decayed completely within about 6H downstream because of the “suburban” type atmospheric boundary layer. In Castro and Robins (1977) case of an incidence angle at 45°, measurements indicate that in uniform flow the near wake and pressure field are dominated by strong vortices shed from the top edges of the body. The vortices have a marked effect on the axial component of velocity, but that the velocity appears to decay quite rapidly (Castro & Robins, 1977). The velocity component beyond about 6H downstream are very similar to those behind a cube normal to the flow. The results show that the downwash behind the obstacle is greater for an incidence angle for 45° than for 0°. This shows that the vorticity decays almost as rapidly as the rest of the wake (Castro & Robins, 1977). They point out that for the rate at which the velocity deficit and the swirling motions decay can be very different and that further experimental work is necessary to quantify these differences.

3 METHOD

In this chapter WindSim in general will be described with focus on the primarily used features in this thesis. First a short description will be presented, and further the importance of grid resolution, boundary conditions, climatology, wind fields, wind resources, calculation of AEP and at last the most important feature used; the blocking file. A more thoroughly description of how the different methods are utilized in both the wind tunnel experiment and at Borg Havn is presented in chapter 4 and 5. This as well as the setup for each study will be described in detail in the same chapters.

3.1 WINDSIM

WindSim is a CFD-based wind farm design tool with many features for wind analysis. It is bases on a three-dimensional Reynolds Averaged Navier Stokes (RANS) equation (WindSim, 2019). Experimental data from a limited area is used in a numerical model to assess the wind resources within a larger area. The numerical model calculates the terrain-induced acceleration of the wind field by solving the non-linear transport equations for mass, momentum and energy wakes (WindSim, 2019). WindSim is a suitable tool for simulations in both complex terrains, and in situations with complex local climatology (WindSim, 2019).

3.1.1 HOW IT WORKS

WindSim is dependent on many different inputs and factors. Local topography highly influences local wind fields (WindSim, 2019). The inputs in WindSim is based on a digital terrain model (DTM), a gws-file, in a proper length scale according to the phenomenon to be investigated. With the DTM established, a similar model with terrain roughness must be supplied. On the zone towards ground the terrain roughness has a particular impact (WindSim, 2019). Finally, Meteorological data is the next input WindSim needs. At least on point within the modeled area must be provided (WindSim, 2019). With these primary inputs, the following wind resources for the whole area can be calculated. The annual energy production (AEP) from any number of wind turbines can also be calculated.

3.1.2 TERRAIN AND ROUGHNESS

To start the simulations in WindSim, the first step is to run the terrain module. When a project is going to be started a gws-file is generated which contains elevation and roughness data in a regular grid (WindSim, 2019). A global or local coordinate system is chosen, and after generating the 3D model an extension can be utilized to make the grid smaller and to fit the area of interest.

A refinement area can also be chosen. By default, WindSim don't generate a grid at ground plane (WindSim, 2019). Here the mentioned extension is chosen in the bws-file and a refinement within the extension can be chosen. The refinement area is normally uniform distributed around the area of interest but can be modified to fit the area of interest. In the same bws-file the blocking file feature is also utilized, further explained in section 3.1.9. To obtain accurate numerical solutions the distribution of nodes in the vertical direction should be as dense as possible, mainly near the ground (WindSim, 2019). The generated 3D model will consist of $nx * ny * nz$ cells, which can be chosen in the settings as maximum number of cells, or generated through the chosen number of cells in the bws-file (WindSim, 2019). In Figure 3.1 an example of a refinement around the center of the grid is shown.

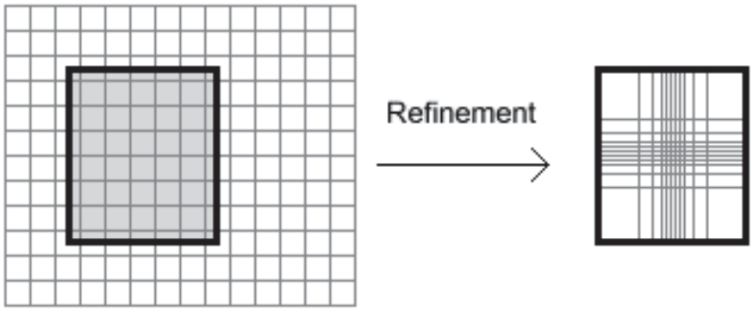

Figure 3.1: An example of a refinement of a grid (WindSim, 2019)

3.1.3 GRID RESOLUTION

The grid resolution is maybe one of the most important factors regarding a sufficient simulation in WindSim. Height and roughness information from a specified grid is needed to utilize the numerical model and the accuracy of the simulation is highly dependent on the resolution of the grid (WindSim, 2019). For a meso-scale modeling a typical resolution in the order of 100x100m is used within larger areas in the order of 1000x1000km (WindSim, 2019). A finer resolution in the order of 10x10m is necessary for micro scale modelling (WindSim, 2019).

The conditions are shown in Figure 3.2 with a mountain where half of the points used in the discrete representation have successively been removed. At the left you can see this with a 25m point spacing, and on the far right the same mountain with a 200m point spacing is shown. An obstacle or building would look mostly the same, although with a different shape, but the idea is the same.

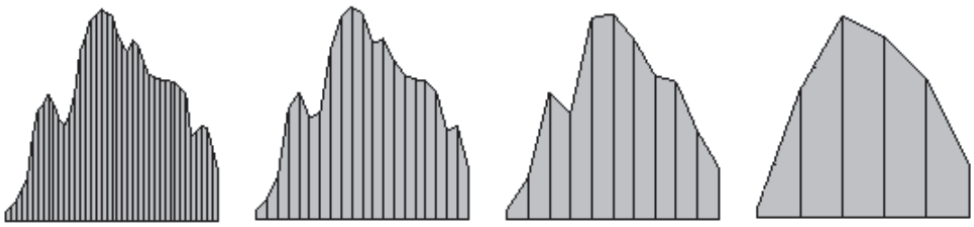

Figure 3.2: Discrete terrain with successive removal of points (WindSim, 2019)

As a result of the grid resolution the wind resources will be highly dependent on the chosen number of cells (WindSim, 2019). In the figure below a wind field above an island with an extension of the model with 3500x3800m grid resolution is shown. With the modest topography on the island shown in Figure 3.3 on the lower left with the grid resolution on 25x25m shows a highly more detailed wind resource map than with 200x200m

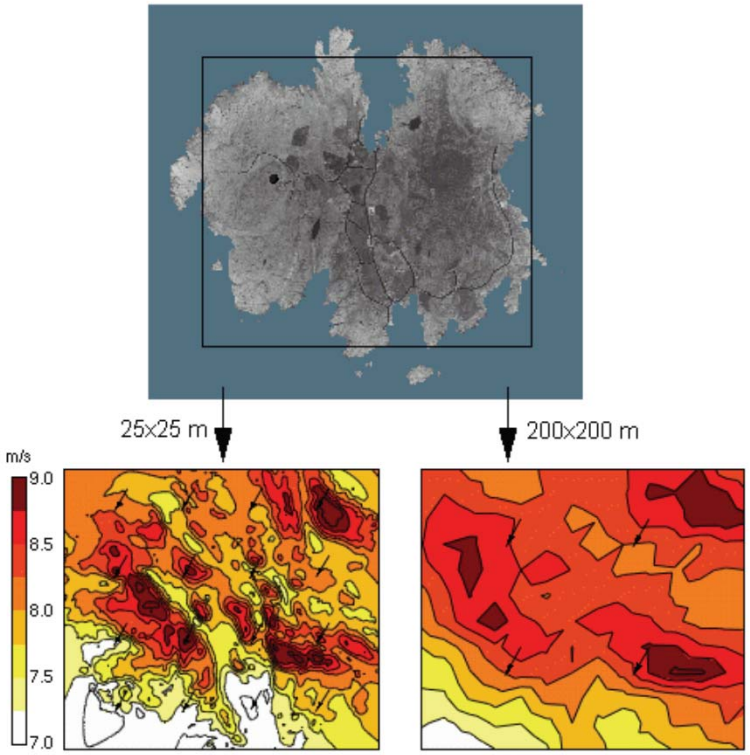

Figure 3.3: Wind fields for different grid resolutions (WindSim, 2019)

3.1.4 Boundary conditions

A 3D computational domain is used for the numerical model for simulations (WindSim, 2019). Information about the flow field must be supplied along the border of the computational domain (WindSim, 2019). The boundary conditions are given as fully developed flow profiles taking into account the given roughness at the border. On the other hand, the model will not have any information about the wind field outside the computational domain (WindSim, 2019). Any sudden changes in topography or roughness along the border will influence the flow field. To reduce this problem, a border zone where the flow field is allowed to adapt to the surroundings is introduced (WindSim, 2019). In this zone no results are presented. In some cases, there might be impossible to avoid areas with sudden changes in the mentioned factors along the border, these areas should be treated with caution (WindSim, 2019).

3.1.5 Climatology

A meteorological input is highly crucial for the quality of the numerical results (WindSim, 2019). To represent the long-term wind climate in the area of interest based on meteorological data collected during a short time interval, these data must be correlated to long-term nearby statistical data. It is also important that the data is representative for the whole computational area (WindSim, 2019). Further on, the data must be compatible with the scale of the numerical model. A meteorologically input has to at least be supplied for on point within the modeled area (WindSim, 2019). This factor is again highly important, and the increase in amount of data will of course improve the accuracy of the numerical results (WindSim, 2019). In this case study at Borg Havn a transferred climatology was used, which is a source to uncertainties.

3.1.6 WIND FIELDS

By solving the Reynolds Averaged Navier-Stokes equation the wind fields at the chosen location can be determined. A number of turbulence models can be chosen, but the standard k-ε model, which is used in this study, is set as default. By starting with the initial conditions chosen, which are guessed estimations, the solution is progressively resolved by the chosen value of iterations (WindSim, 2019). The flow variables that are solved is pressure, velocity component, turbulent kinetic energy and turbulent dissipation rate (WindSim, 2019). The roughness height highly influences the vertical profiles extracted, which is done in the wind tunnel experiment. The stability of the atmosphere will also influence this, and in the case of a neutral atmosphere the wind profiles are logarithmic (WindSim, 2019).

The residuals and numerical errors for the wind field simulations in are monitored, and when they reach a given edge, a converged solution is obtained (WindSim, 2019). When the wind speed and turbulent variables, as well as the spot values, have settled, convergence has been obtained and indicate that the simulations will not change from one iteration to the next (WindSim, 2019).

Some important settings are utilized to make a sufficient simulation of the wind fields. Firstly you have the height of the boundary layer which the wind profile is defined from the ground and up to the boundary layer height, which the profile is constant above this height (WindSim, 2019). Second is the boundary condition at the top of the boundary layer which can be set to either “fixed pressure” or “no-friction wall”. For complex terrain the “fixed pressure” condition should be used and over flat terrain the “no-friction wall” is used (WindSim, 2019). Third setting which is important is the number of iterations. This setting will depend on the number of cells (WindSim, 2019). Lastly, the convergence criteria must be set. This setting influences when the simulations can be stopped automatically when a certain level of convergence is reached (WindSim, 2019). The default value is set to 0.005, which will be used in this thesis.

3.1.7 Wind resources

To run the wind resource module at least one climatology must be present as well as all sectors from wind fields have been calculated. By weighting the wind database against the climatology, the wind resource map is established (WindSim, 2019). Heights above ground level which the wind resource map needs to be extracted has to be chosen. Due to terrain effects the wind direction changes in the inner of point the model (WindSim, 2019).Wake effects from the turbines can also be calculated, but in this thesis, this is not utilized. The roughness height is taken from the gws-file constructed under the terrain module, or a constant value can be given (WindSim, 2019).

3.1.8 Annual energy production

The annual energy production (AEP) is calculated for all the visible turbine objects utilizing the chosen climatology (WindSim, 2019). With several climatology's the AEP is calculated separately, which will not be done in this thesis because there is only one climatology chosen in the case at Borg Havn (WindSim, 2019). In this module the vertical profiles can also be exported. The vertical profile file contains several variables, but only the 2D speed will be used in this thesis to compare the vertical profiles.

3.1.9 BLOCKING FILE FEATURE

The most important feature in WindSim for this thesis is the blocking file. To understand this feature we first have to take a closer look on how WindSim utilizes something called refinement. The refinement corresponds to the inner grid at the area of interest. Both the blocking file and refinement feature uses a syntax in a bws-file. The different parameters in the bws-file is given as;

- i-logical
- j-logical
- k-logical
- junctions
- junctions_obstacle
- surface_obstacle
- volumes_obstacle

In WindSim, when you have loaded in your grid, you check off in the properties for a *Refinement Area* and a bws-file is automatically generated, and the grid will be refined at the center of the global area. An underlying structure of the grid is based on a logical space, with *i* and *j*, as well as *k*. In Figure 3.4 a grid at ground level, *k=1*, is shown with 4 junction points in the logical space in both *i*- and *j*-direction.

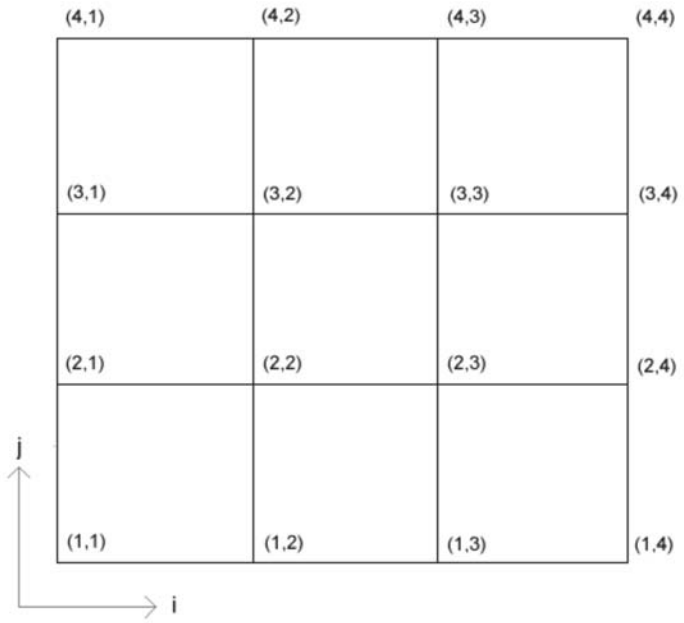

Figure 3.4: A logical space with grid at ground level, k=1 (WindSim, 2019)

Also shown in the figure is that in the logical space the grid at ground level is divided in three logical segments in each direction. Each of these segments has two attributes; a distribution factor and number of inner points along the segment. The latter refers to the inner points, hence the number of cells will be the number of inner points plus one along a line segment. The distribution factor is given from an arithmetic sequence where the value gives the fraction between the first and last cell. An arithmetic sequence is given in general as in equation (3.1) (Piff, 1991). Given a distribution factor of 1 gives equally sized cells.

$$a_n = a_m + (n - m)d \tag{3.1}$$

In the logical space, *k* represents the grid in the physical z-direction, but an addition of one attribute giving the physical extension in the z-direction. To construct the grid by using the logical space, the physical extension and structure of the horizontal plane is given by specifying physical coordinates to all the junction points. The three last keywords in the bws-file are used to specify the obstacle. Here you need to specify the following; the physical grid structure at k-levels larger than 1 for the junctions of the obstacle, surfaces and volumes gives the extension in logical coordinate for blocked 2D surfaces and 3D volumes, and the last one is a type which specify the porosity of the obstacle, where 0 will give a fully blocked solid. To utilize the blocking file and refinement feature you construct a bws-file based on the mentioned attributes. An obstacle is identified by the lines in the logical space. An example with two obstacles constructed in the bws-file is shown in Figure 3.5.

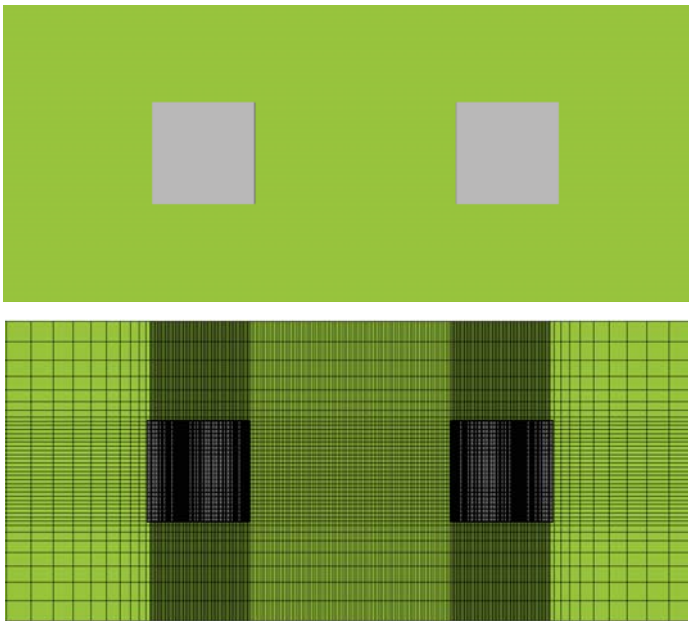

Figure 3.5: An example of two obstacles with corresponding refinement grid

4 Wind Tunnel Experiment

In this chapter the setup and the results from the numerical wind tunnel experiment be presented. The setup includes terrain and roughness, grid setup, wind fields, wind tunnel and obstacle setup, and wind profiles. The results are mainly presented with vertical profiles but are supplemented with cut-planes which shows the different aspects of the flow around the obstacle.

The wind tunnel experiment is based on Castro and Robins (1977) work described in section 2.5.1. Here two different cases, A and B, uniform and logarithmic wind profiles respectively is investigated. The two cases are simulated in a constructed wind tunnel in WindSim with a 1x1x1 geometric block placed downstream of the inlet. The results from Castro and Robins (1977) wind tunnel experiment is compared with the extracted vertical profiles from the wind field simulations. The results are later, in chapter 6, discussed and the cut-planes and vertical profiles are compared to the reviewed literature in section 2.5.1.

4.1 Numerical Setup

4.1.1 Terrain and roughness

In Figure 4.1 the terrain elevation and roughness are shown. As indicated in the figure, the elevation in the wind tunnel is zero. Also shown in the right figure, the roughness is equal to 0.03 m.

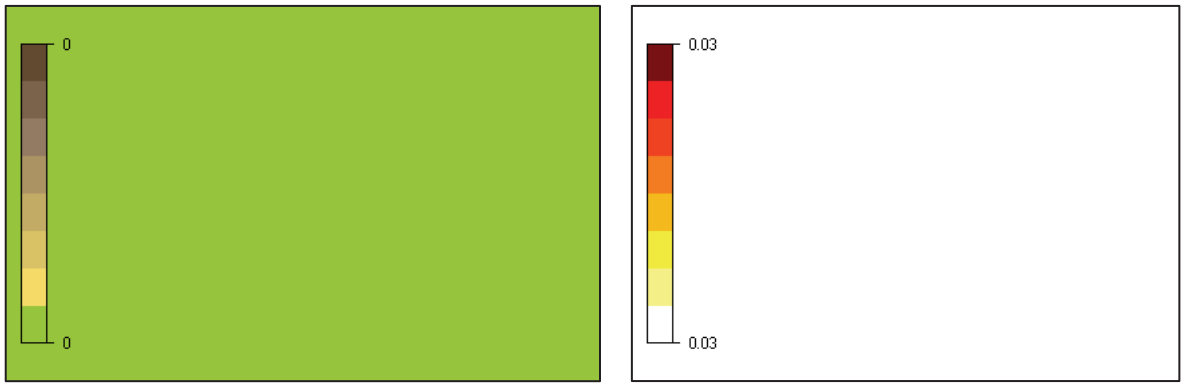

Figure 4.1: Terrain elevation and roughness respectively

4.1.2 OBSTACLE

In Table 2 the blocking file setup for constructing the obstacle is given. Here you can see the distribution factor and number of points. This as well as the number of junction points used, which ended up at 16 in i- and j-direction, and 3 in k-direction. In the k-direction a distribution factor of 1 were chosen for the cells up to 1m, the height of the obstacle, and above this 0.1. The distribution factor for i- and j-direction were set so the distribution was equal in front and behind the obstacle, but a uniform distribution was chosen for the obstacle area.

Table 2: Blocking file setup

```
i-logical          :    line_i  points   distribution
                              1      20    7.4615
                              2      29    1.0000
                              3      40    0.1340

j-logical          :    line_j  points   distribution
                              1      20    5.8000
                              2      29    1.0000
                              3      20    0.1724

k-logical          :    line_k  points   distribution  z_upper
                              1      29    1.0000        1.0
                              2      30    0.1000        5.0

junctions          :         i       j       k  co-ord          x  |          y          z
                             1       1       1       3        0.0000       0.0000       0.0000
                             2       1       1       3        2.0000       0.0000       0.0000
                             3       1       1       3        3.0000       0.0000       0.0000
                             4       1       1       3       10.0000       0.0000       0.0000
                             1       2       1       3        0.0000       2.0000       0.0000
                             2       2       1       3        2.0000       2.0000       0.0000
                             3       2       1       3        3.0000       2.0000       0.0000
                             4       2       1       3       10.0000       2.0000       0.0000
                             1       3       1       3        0.0000       3.0000       0.0000
                             2       3       1       3        2.0000       3.0000       0.0000
                             3       3       1       3        3.0000       3.0000       0.0000
                             4       3       1       3       10.0000       3.0000       0.0000
                             1       4       1       3        0.0000       5.0000       0.0000
                             2       4       1       3        2.0000       5.0000       0.0000
                             3       4       1       3        3.0000       5.0000       0.0000
                             4       4       1       3       10.0000       5.0000       0.0000

junctions_obstacle :         i       j       k  co-ord       x         y         z

surfaces_obstacle  :       i_s     i_e     j_s     j_e     k_s     k_e    type

volumes_obstacle   :       i_s     i_e     j_s     j_e     k_s     k_e    kind    type      c1      c2
                            2       3       2       3       1       2    obstacle  0.0     0.0     0.0
```

4.1.3 GRID SETUP

The grid was setup with 85, 110 and 50 in x-, y- and z-direction respectively. This gives a total of 467 500 cells. How the bws-file was constructed to set up the grid and obstacle, as well as number of cells and distribution factor is shown in Table 2 in section 4.1.2. In Table 3 the grid setup is given.

Table 3: Grid setup

	x	y	z	Total
Grid spacing: min – max (m)	2.1 – 127.7	1.5 – 147.6	Variable	-
Number of cells	85	110	50	467500

In Figure 4.2 the grid with the obstacle is shown in 3D. While Figure 4.3 shows the grid in xy-plan. Figure 4.4 shows the grid in z-direction.

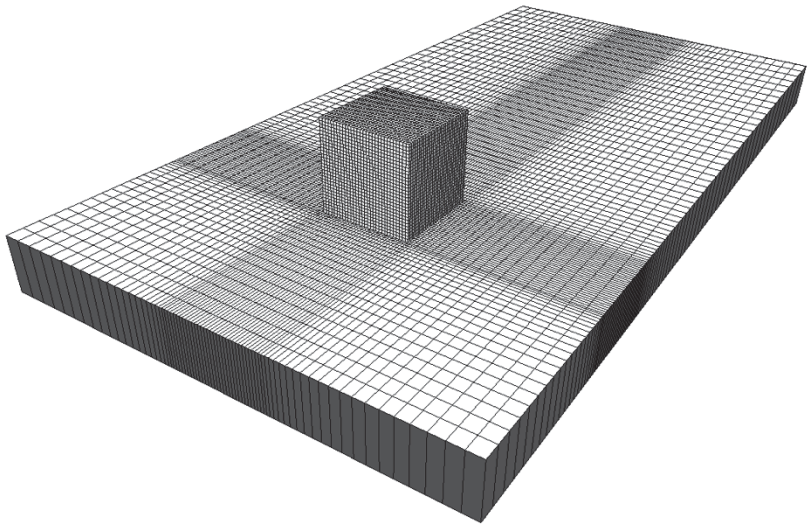

Figure 4.2: The grid with obstacle

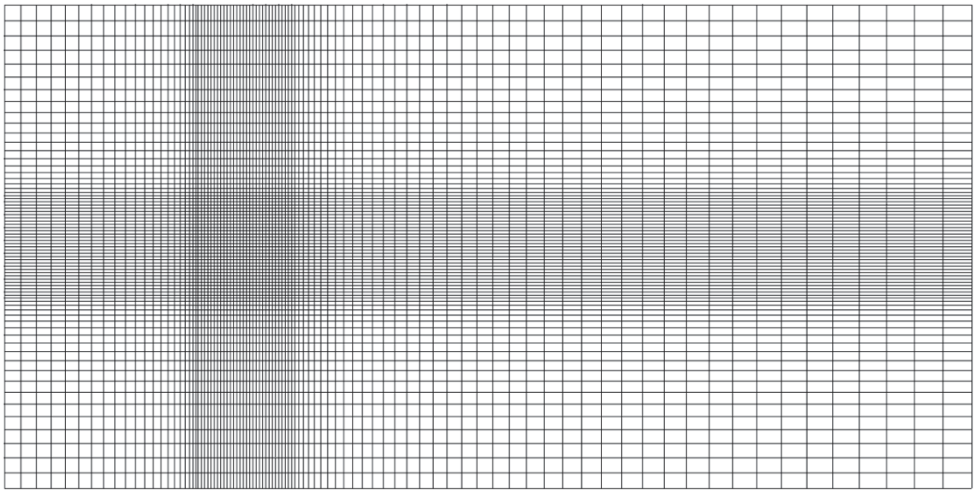

Figure 4.3: Grid in xy-direction

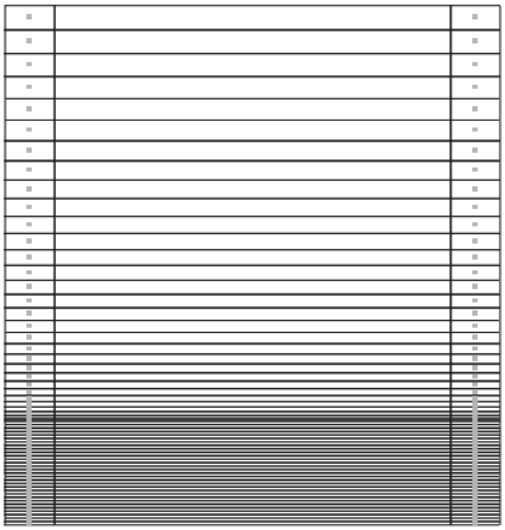

Figure 4.4: Grid in z-direction

4.1.1 WIND FIELDS

In Table 4 the solver settings for the wind field simulations are given. The height of the boundary layer was set to 5m, equal to the height of the wind tunnel. The speed above the boundary layer was set to 1 m/s to make the measurements dimensionless. A standard k-ε turbulence model was used. The convergence criteria were set to 0.005 which make the simulation stop as it reaches this certain level of convergence. For the boundary conditions at the top a "no-friction wall" setting was used because of the flat terrain in the wind tunnel.

Table 4: Solver settings for Case A and B

Height of boundary layer (m)	5.0
Speed above boundary layer (m/s)	1.0
Boundary condition at the top	fix pres.
Potential temperature	No
Turbulence model	Standard k-epsilon
Solver	GCV
Maximum iterations	500
Convergence criteria	0.005
Boundary conditions at top	No-friction wall

The number of iterations it took for the wind field calculations to converge was 235, shown in Table 5 for Case A and 119 for Case B shown in Table 6. In Figure 4.5 and Figure 4.6 the residual- and spotvalues is shown for Case A and B. The graphs show that in both cases the simulations converge.

Table 5: Simulation time, number of iterations and convergence status Case A

Sectors	Simulation time	Iterations	Status
270	00:53:49	235	C

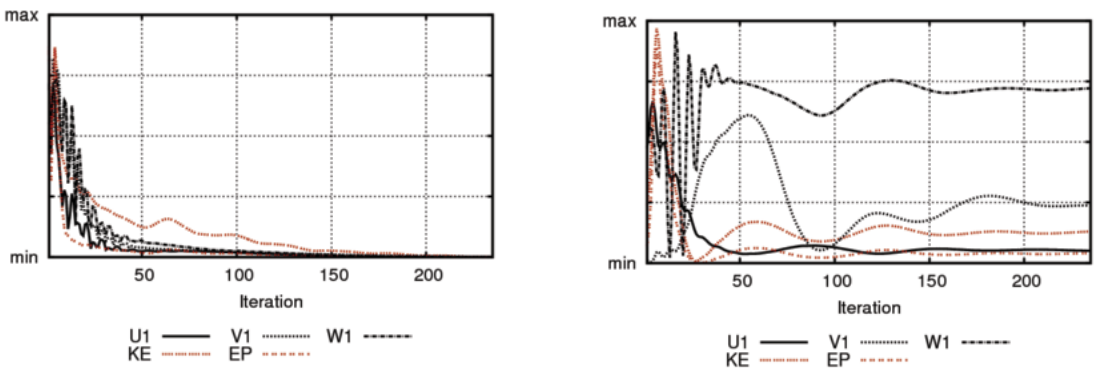

Figure 4.5: Residual values and spotvalues from convergence study of wind field simulations for Case A

Table 6: Simulation time, number of iterations and convergence status for Case B

Sectors	Simulation time	Iterations	Status
270	00:28:20	119	C

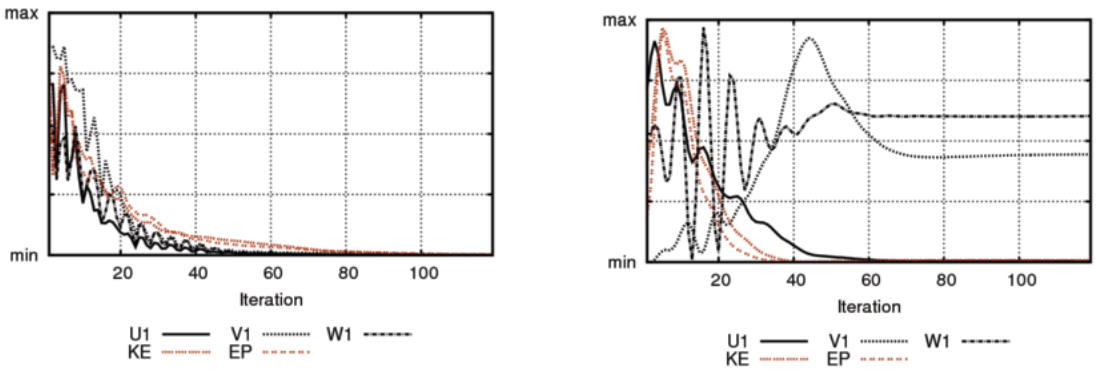

Figure 4.6: Residual values and spot values from convergence study of wind field simulations Case B

4.1.2 WIND TUNNEL SETUP

The wind tunnel was set up with the dimensions of 10x5x5m. The obstacle with dimensions 1x1x1m was placed 3m downstream of the inlet. The setup is shown in Figure 4.7 with the axes for the obstacle, which is different from the wind tunnel axis. 0 is in the center of the obstacle.

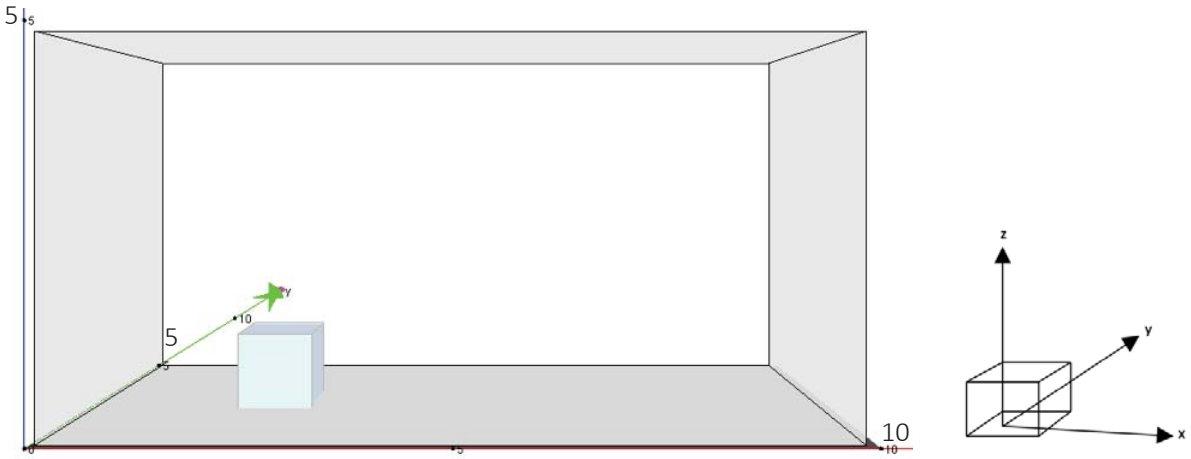

Figure 4.7: Wind tunnel setup with dimensions in meters and the local axis for the block on the right

In Figure 4.8 the point for extractions of numerical results is shown. A total of 6 points were chosen to make sufficient results, in addition the inlet was measured for comparison with the outlet.

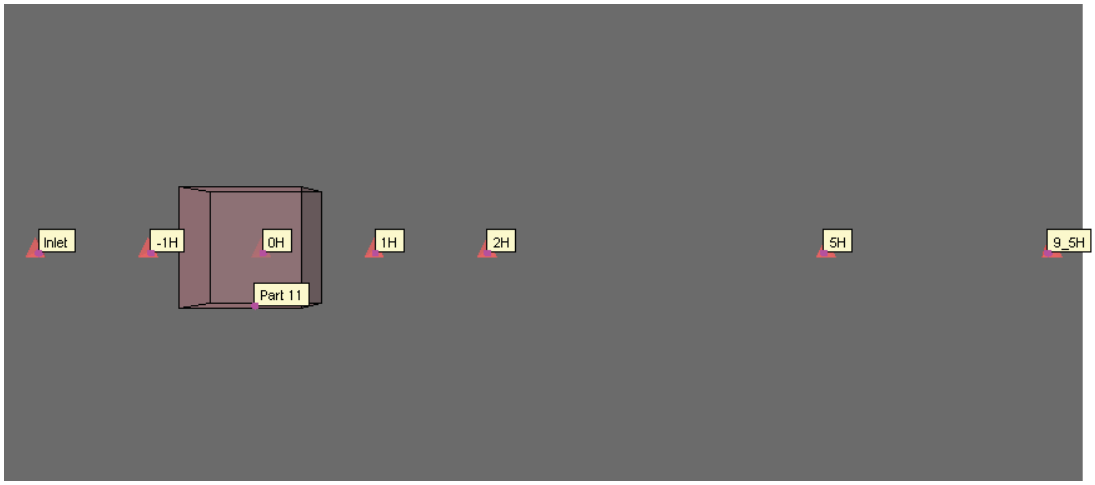

Figure 4.8: Measurement locations with corresponding distance related to the height of the obstacle

4.1.3 WIND PROFILES

The two different cases, A and B, is as mentioned based on Castro and Robins (1977) work. Case A which is a uniform distributed wind profile is shown in Figure 4.9, and Case B, a logarithmic distributed wind profile, is shown in Figure 4.10.

WindSim is not mainly used with a uniform wind profile. To tweak the software to utilize such a profile, a modification had to be done. There exist a Q1-file in the software which can be modified. Here the wind profile was set to use a uniform distributed wind profile

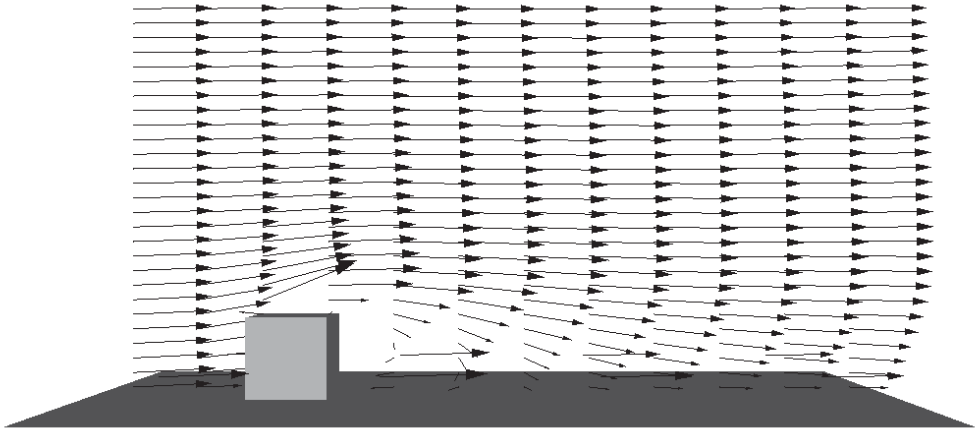

Figure 4.9: Uniform distributed wind profile (Case A)

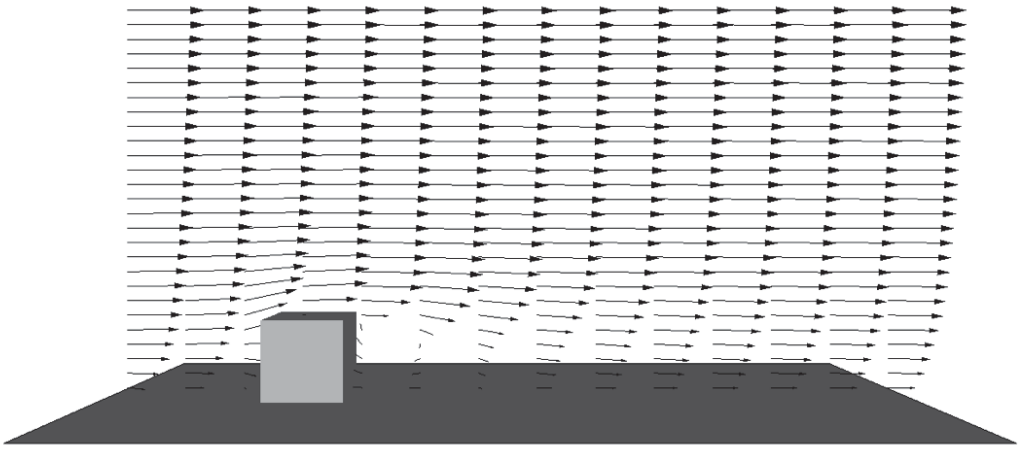

Figure 4.10: Logarithmic wind profile (Case B)

4.2 Results

4.2.1 Case A

In Figure 4.11 the vertical cut plane in yz-direction at $x = 0$ is shown with a maximum wind speed of 1 m/s. The figure indicates that for the uniform wind profile there is no noticeable effect around the sides of the obstacle, although there is some indication of reduced wind speed on the sides and at the top.

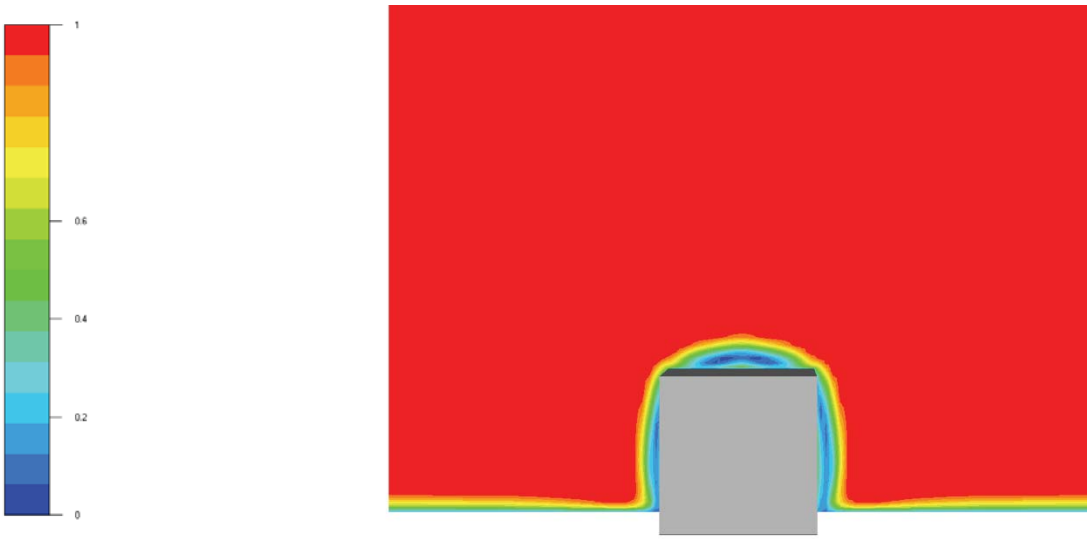

Figure 4.11: Vertical cut plane in yz-direction at x=0, legend in m/s

In Figure 4.12 the horizontal cut plane is shown for the xy-direction at $z = 0$. Here, there is a larger and more noticeable effect on the flow around the obstacle. In the front there occur a suction area with decreasing wind speed, as well as a slight effect going further out on the sides. On the sides of the obstacle the wind speed is below 0.2 m/s closest to the walls, and the wind accelerates out on the sides. Behind the obstacle the most noticeable effects occur. Firstly, the blue region indicates a reduced wind speed of about 0.3 m/s and below. It occurs a recirculation area with higher wind speeds, indicated by light blue, closest to the backside of the obstacle. Also, two regions with 0 m/s occur behind the obstacle, which can indicate a recirculation area with actual negative wind speeds. The wind speed restores increasingly behind the obstacle downstream, but never reattaches fully in the simulated wind tunnel.

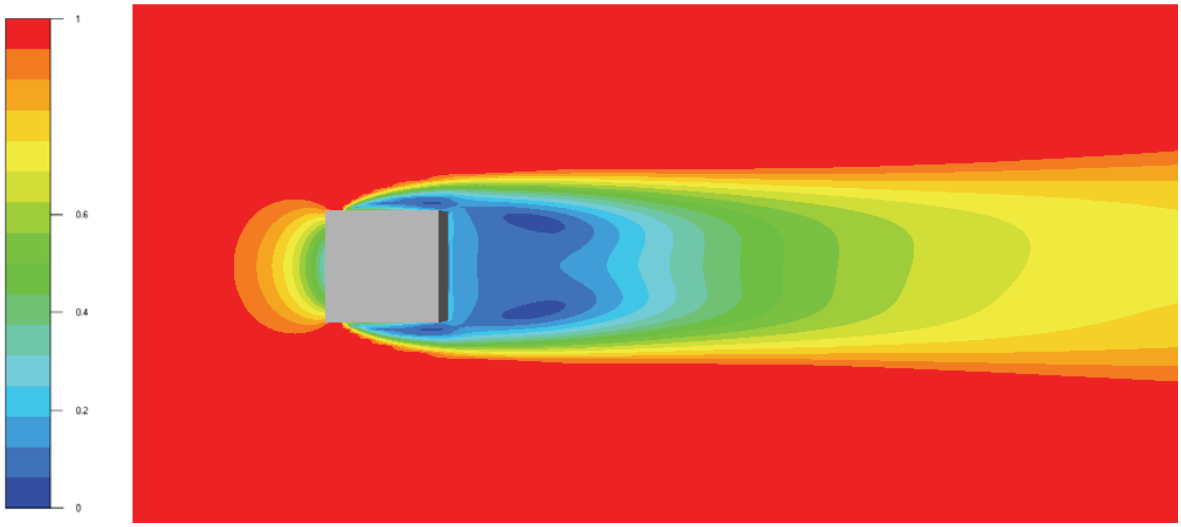

Figure 4.12: Horizontal cut plane in xy-plane at z=0, legend in m/s

For the vertical cut plane for the xz-plane at $y = 0$ is shown in Figure 4.13. In the front, the same suction area which was indicated in the horizontal cut plane occurs. The flow on the top surface of the obstacle increases in height related to the length of the obstacle. In the vertical cut plane, the recirculation area with occurring eddies is better shown than in the horizontal cut plane. Here you can see a region of wind speeds of 0.3 m/s close to the floor of the wind tunnel, while higher up, about 2/3H, there exists a region of 0 m/s. The wind reattaches downstream about 3-4H from the obstacle.

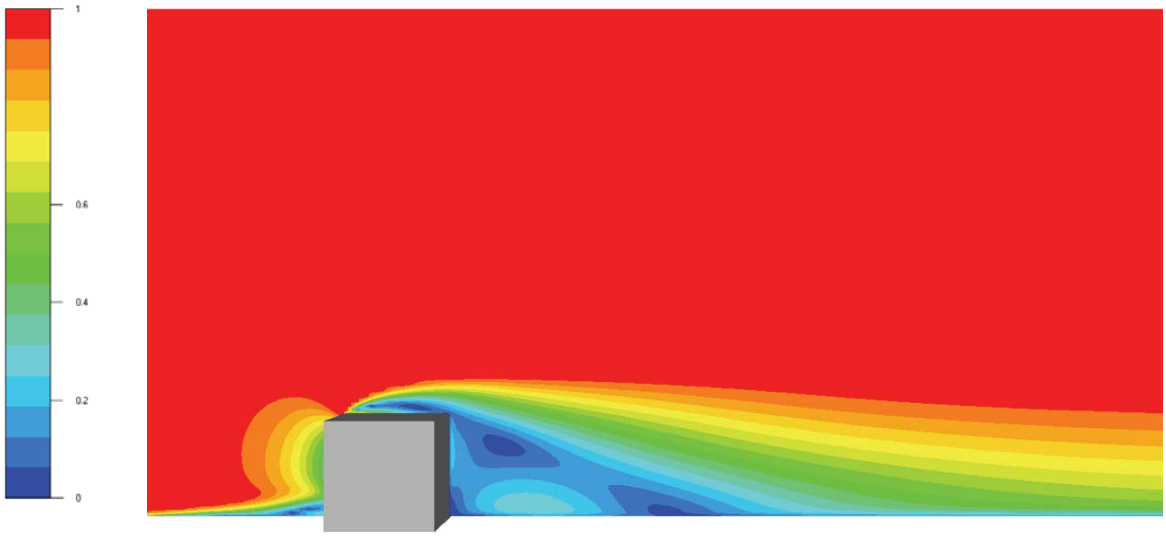

Figure 4.13: Vertical cut plane in xz-plane at y=0, legend in m/s

In Figure 4.14 and Figure 4.15 vector fields in horizontal and vertical view is shown at $z = 0$ and $y = 0$ respectively. Here the mentioned recirculation areas are better shown. The blue vectors indicate a reversed flow behind the obstacle extending to about 2H, this is best shown on the vertical vector field.

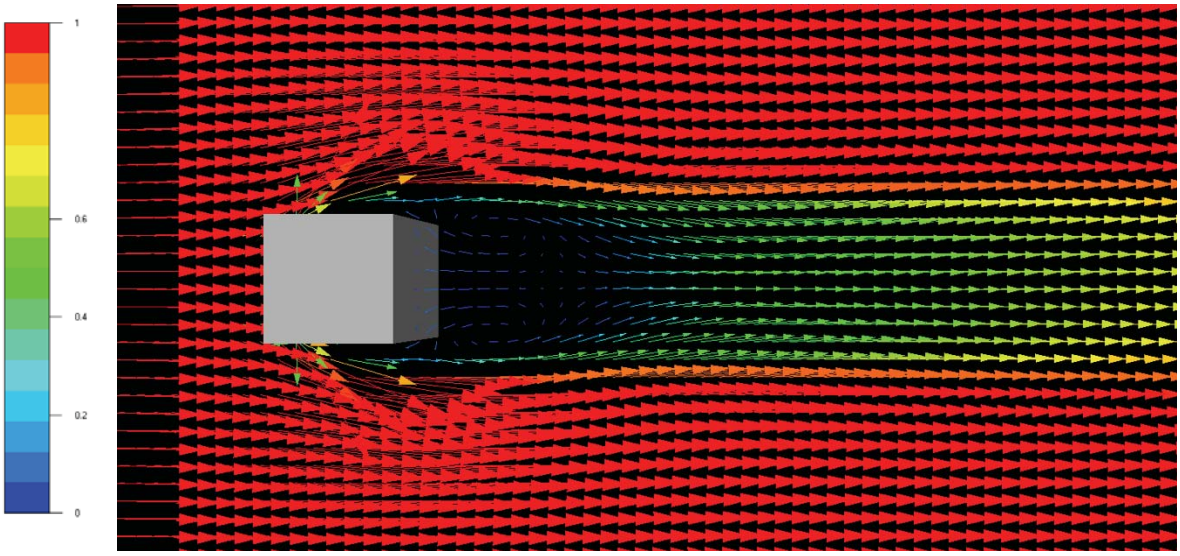

Figure 4.14: Horizontal vector field 3D velocity at z=0, legend in m/s

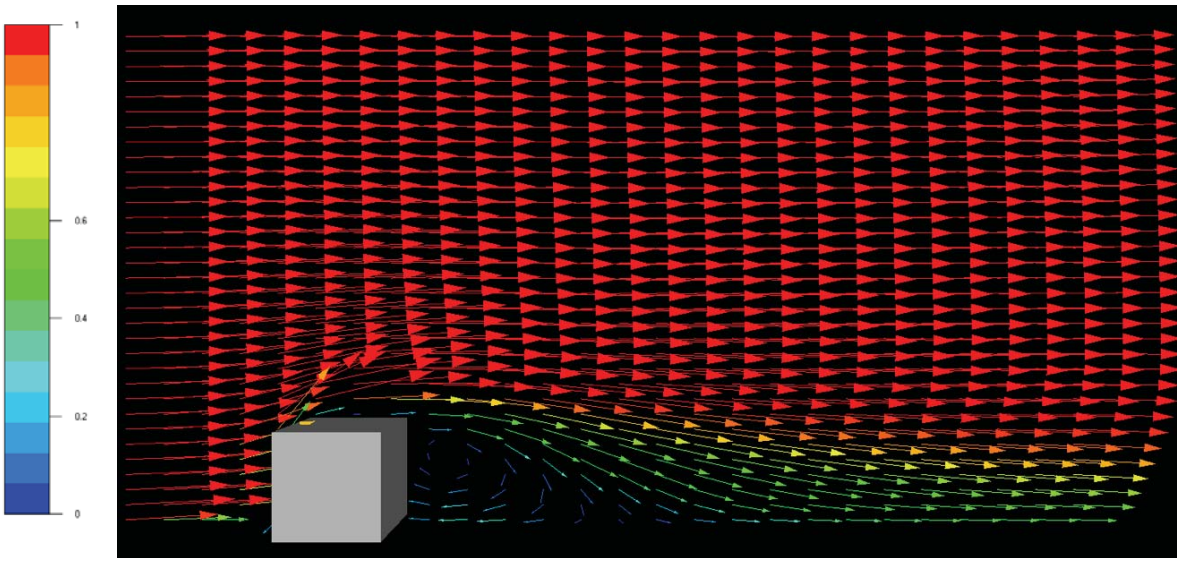

Figure 4.15: Vertical vector field at y=0, 3D velocity, legend in m/s

4.2.2 CASE B

Figure 4.16, Figure 4.17 and Figure 4.18, show the vertical cut plane for yz-plane at $x = 0$, horizontal cut plane for xy-plane at $z = 0$ and vertical cut plane for xz-plane at $y = 0$ respectively. Here the logarithmic wind profile is shown by the increasing wind speed to the top of the boundary layer, in difference from Case A which had a uniform profile. For the horizontal profile there is nearly the same results as in Case A, the only difference is the mentioned increasing wind speed.

Figure 4.16: Vertical cut plane for yz-plane at x=0, legend in m/s

From a horizontal point-of-view you can see a shorter, around 1H, recirculation area comparing with Case A. Also, the wind speed reattaches around 5H behind the obstacle which is a major difference from Case A, which never reattach.

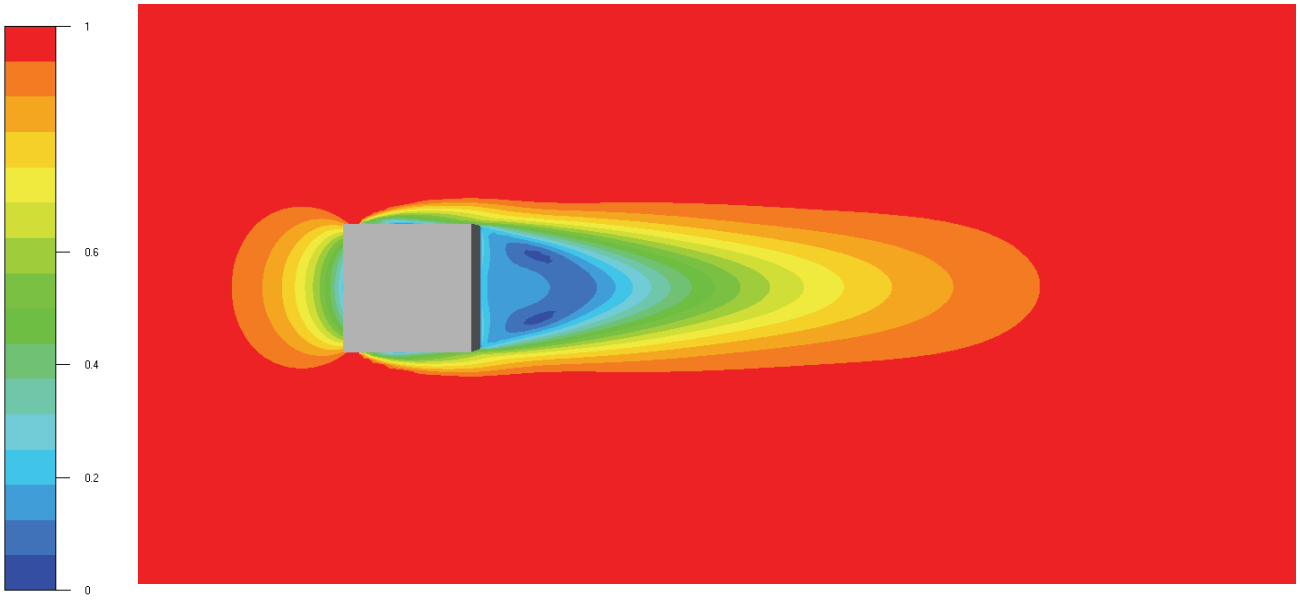

Figure 4.17: Horizontal cut plane xy-plane at z=0, legend in m/s

In the vertical cut plane for the xz-plane a larger area with 0 m/s occur compared with Case A, as well as a larger area with zero wind speed. Although the recirculation area is larger, it does not extend as far as in Case A. The flow on the top of the obstacle extends further than in Case A.

Figure 4.18: Vertical cut plane for xz-plane at y=0, legend in m/s

In Figure 4.19 and Figure 4.20 the vector field is shown in horizontal and vertical view. Remark that the legend is from 0 to 0.65 m/s in difference from the other presented cut planes. They show the same as in the cut planes, and the recirculation area occurs with recirculating vectors behind the obstacle.

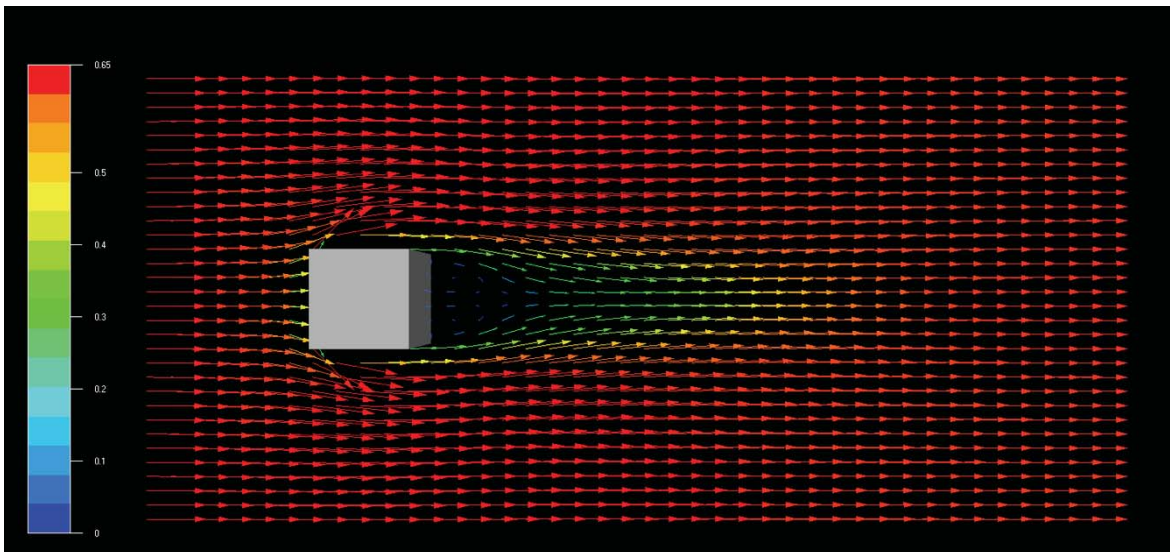

Figure 4.19: Horizontal vector field at z=0 for 3D velocity, legend in m/s

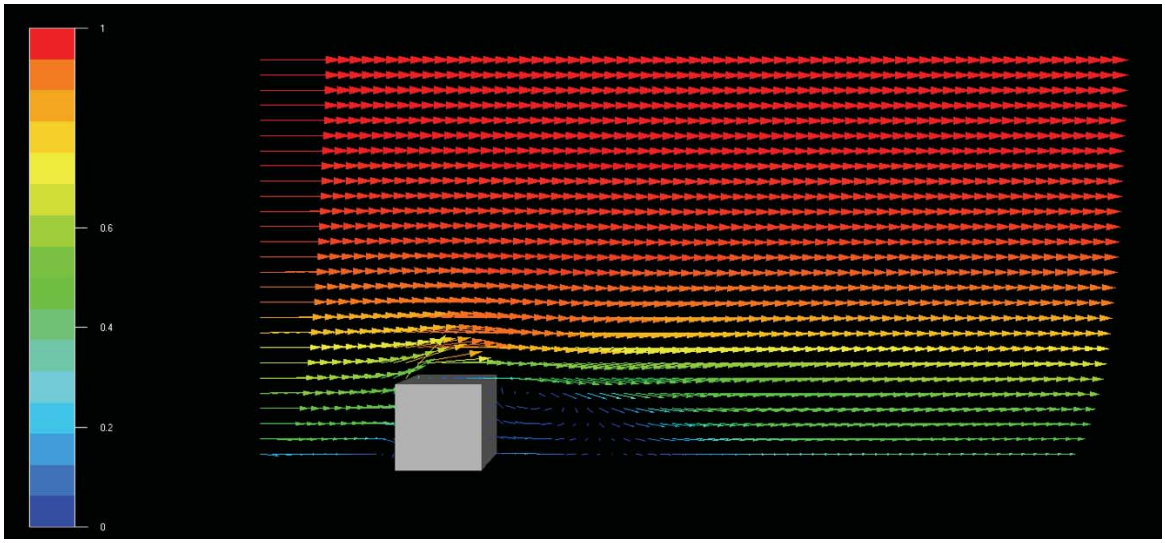

Figure 4.20: Vertical vector field at y=0 for 3D velocity, legend in m/s

4.2.3 VERTICAL PROFILES

The vertical profiles are shown in the following figures at $y = 0$. Figure 4.21 show the inlet of Case A and B compared. They clearly show a uniform and logarithmic wind profile. It is uncertain why there is a skewed dip on Case B, but this might be to a slight weakness for the setup in WindSim since it is not usually used with a uniform distributed wind profile. Different measurements were utilized according to what was described in 4.1.1, ranging from -1H to 9.5H. It is important to mention that the axes are dimensionless. Figure 4.31 and Figure 4.32 show a comparison between the inlet and outlet at 9.5H to see when the wind reattaches. As you can see from the different figures they correspond well with what Castro and Robins (1977) found although some small differences can be seen. It is important to mention that WindSim could not generate negative wind speeds, so the figures that show a negative wind speed from Castro and Robins (1977) results are the same as the reduction in wind speed from WindSim indicated by a reversed graph. This as well indicates the recirculation area. Although the wind tunnel is 5H high, Castro and Robins (1977) only had measurements up to 3H.

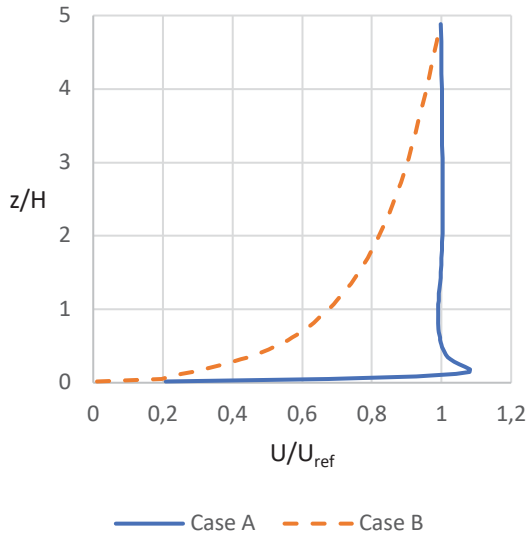

Figure 4.21: Inlet profiles of Case A and B

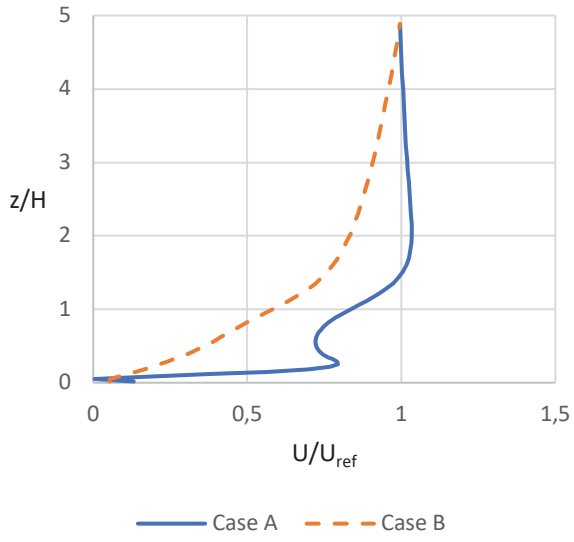

Figure 4.22: Case A vs Case B at -1H

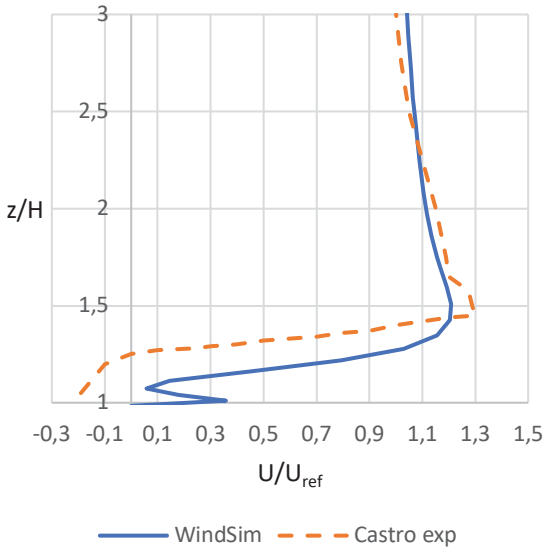

Figure 4.23: Case A at 0H

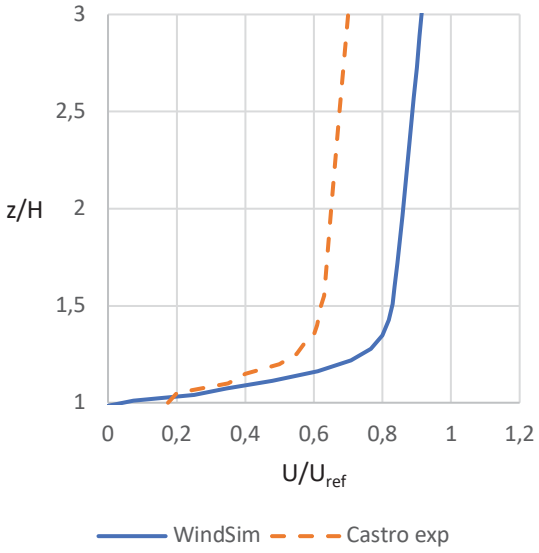

Figure 4.24: Case B at 0H

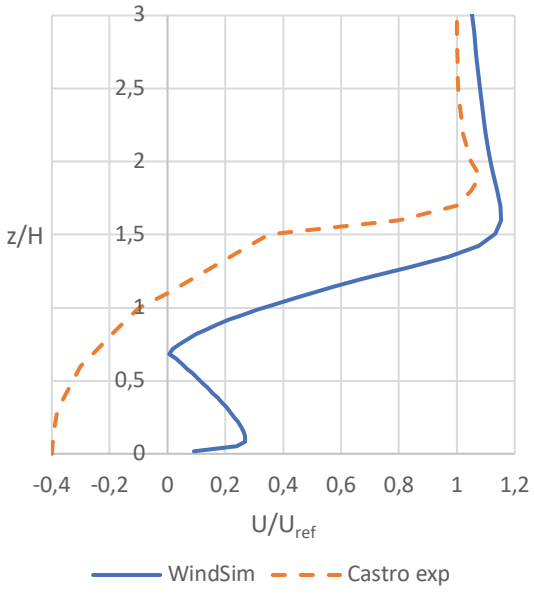

Figure 4.25: Case A at 1H

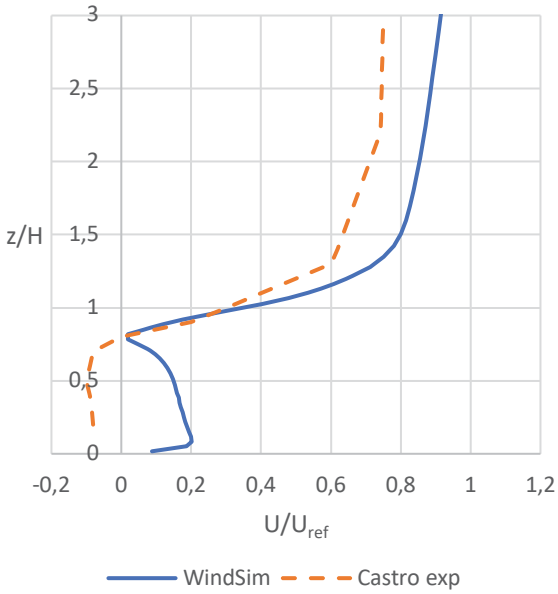

Figure 4.26: Case B at 1H

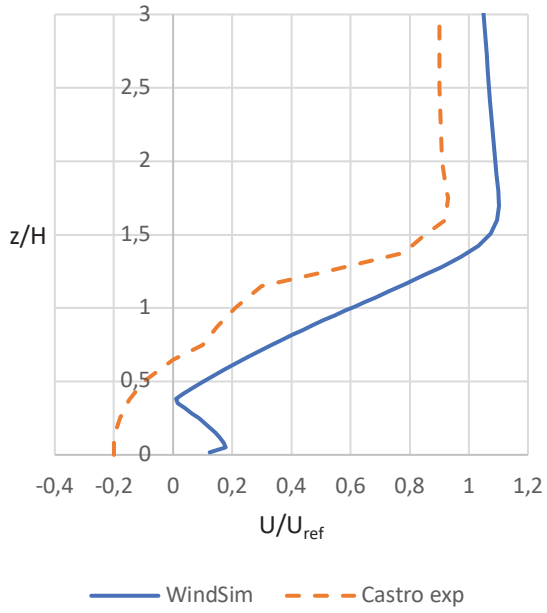

Figure 4.27: Case A at 2H

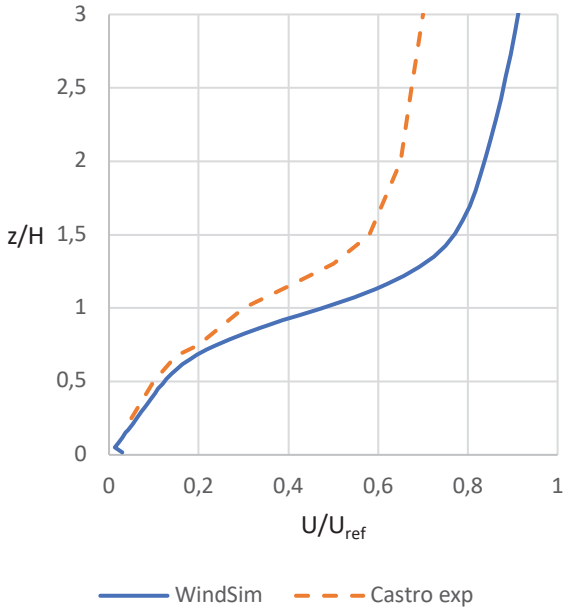

Figure 4.28: Case B at 2H

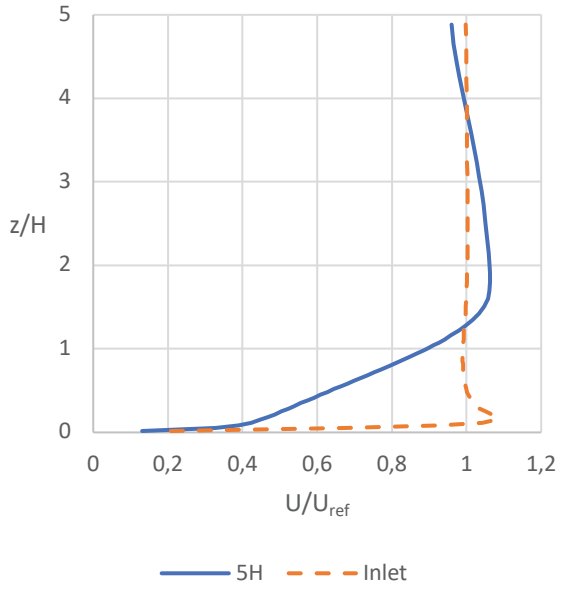

Figure 4.29: Case A comparison between the inlet and distance 5H

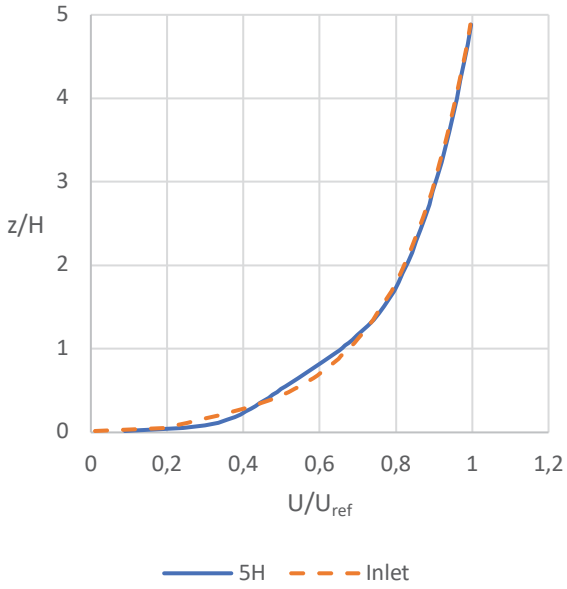

Figure 4.30: Case B comparison between the inlet and distance 5H

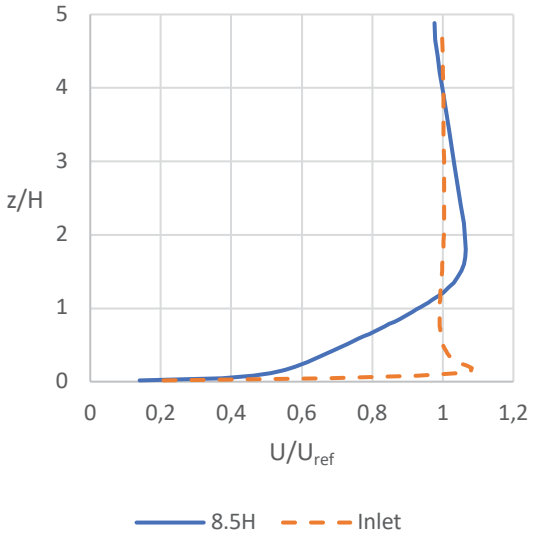

Figure 4.31: Case A comparison between the inlet and outlet at 8.5H

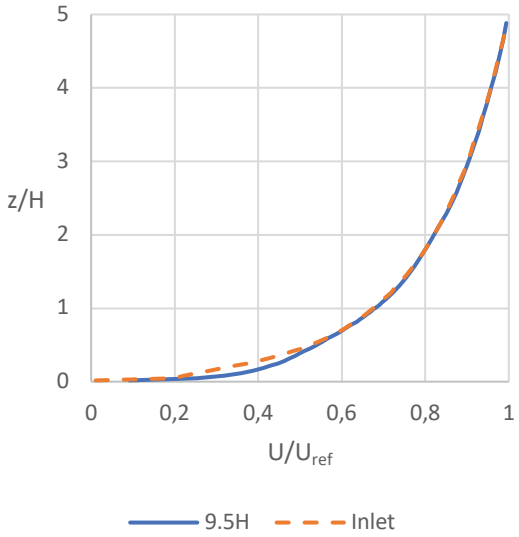

Figure 4.32: Case B comparison between the inlet and outlet at 9.5H

5 Case Study – Borg Havn

5.1 Background

Borg Havn is located in the eastern part of Norway in Fredrikstad. It is a major port with daily activity ranging from deliveries for NATO-rehearsals and shipment all over the world. This makes it one of the busiest arrival points for ships in Norway. They have an ambition on being a total emission-free port by 2030. Also, they want self-supplied energy for their different energy demanding machinery such as cranes, vehicles and supply of green energy to the ships moored. As well as this, they want to be in front going into the activity on new energy- and environmental-solutions in port areas. In collaboration with Smart Innovation Norway they want to actively support network building and to study self-produced energy. They want to participate in the renewal of machinery park to emission-free vehicles and machines. They want to utilize the energy efficiently through local energy production, energy sharing, power saving and the best possible design of a port terminal. Another important aspect is to develop a redundancy in the port terminal with good back-up solutions for a stabile supply of operations.

5.1.1 LOCATION

Borg Havn is a port located in the east part of Norway in the town of Fredrikstad. It is a major port for ships and industrial process which demand a great amount of energy. In Figure 5.1 the location of the port is shown. The port is located in a shore inlet coming from the southern end of Norway from the North Sea.

Figure 5.1: Location of Borg Havn (Google earth)

5.1.2 Buildings

It is obvious from Figure 5.2 there is quite a lot of buildings which is present at a port of this size. This includes cranes, storage facilities, industrial processes and containers.

Figure 5.2: 3D image of Borg Havn (Google earth)

5.1.3 TURBINE LOCATIONS

They want to utilize the available energy by using a wind turbine located at one of the locations show in Figure 5.3, these are proposed by Borg Havn. Thus, as shown in Figure 5.2, many buildings could possibly affect their foreseen production and potential. Another important factor is that at location E, there is a high storage house under construction that will greatly influence that location. The focus will therefore be on location A and E, later referred to as Turbine A and B respectively, and look at them in relation to the nearby buildings, in combination with the wind resource assessment established by WindSim.

Figure 5.3: Proposed locations of the wind turbine at Borg Havn (Google earth)

5.1.4 WIND RESOURCE ASSESSMENT

The wind resource assessment was established by WindSim AS for Borg Havn on request regarding their pre-project assessment. They used a combination of data from MERRA-2 and local weather stations. They utilized the two nearest MERRA-points, C and D, shown in Figure 5.4 for long-term reference wind analysis (Li, 2018). The three local weather stations, 1, 2 and 3, were selected for short term on-site wind data (Li, 2018).

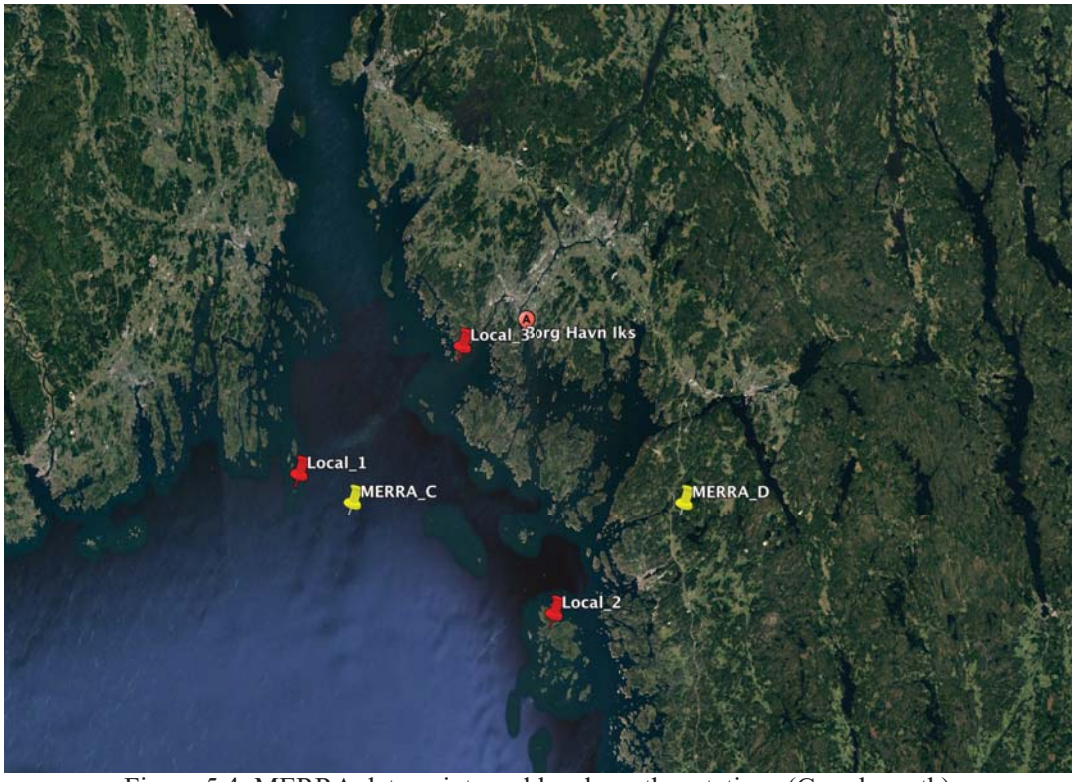

Figure 5.4: MERRA data points and local weather stations (Google earth)

A wind resource map was established based on the above-mentioned data. It is used to identify high wind speed areas based on the average wind speed. For 25m above ground the map is shown in Figure 5.5. It shows that the mean wind speed is around 6.5m/s for most of the Borg Havn at 50m and at 25m between 5.7m/s and 6.1m/s. The wind resources are higher at southern and western parts of the port. The resources are slightly better in the southern and western part of the Borg Havn property and close to the coast at 25m height. Mean wind speeds around 6m/s is dominating. So, the resources are sufficient for the utilization of urban wind energy.

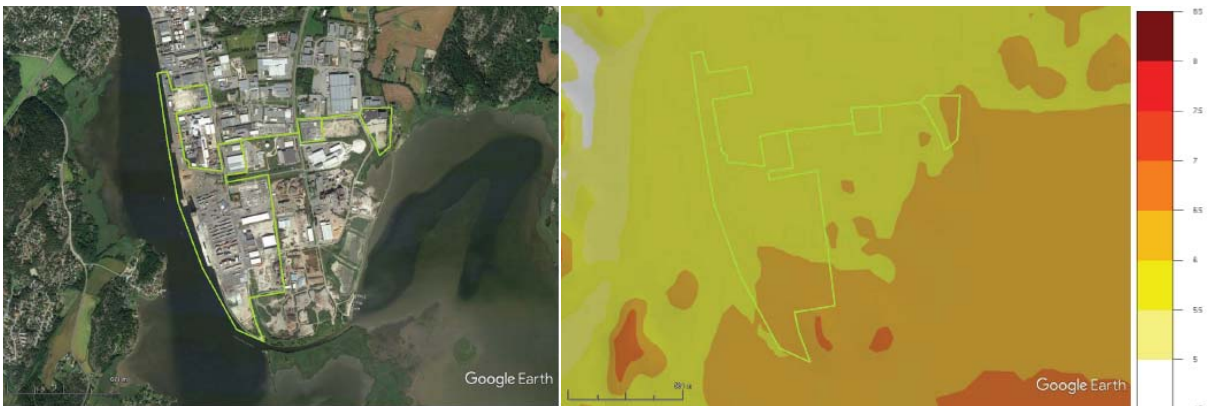

Figure 5.5: Wind resource map at Borg Havn at height 25m (Li, 2018)

For this study climatology point Local_3 were used. To fit the digital terrain model, it was moved closer to Borg Havn, placed at open sea. The average wind speed was measured to 6.21 m/s and dominant wind direction from south-west for this climatology. In Figure 5.6 the wind rose, and Weibull distribution is shown. It also important to mention that the climatology is not representative for the actual wind resources at Borg Havn. This climatology was only utilized to show the differences as a type of dimensionless measure.

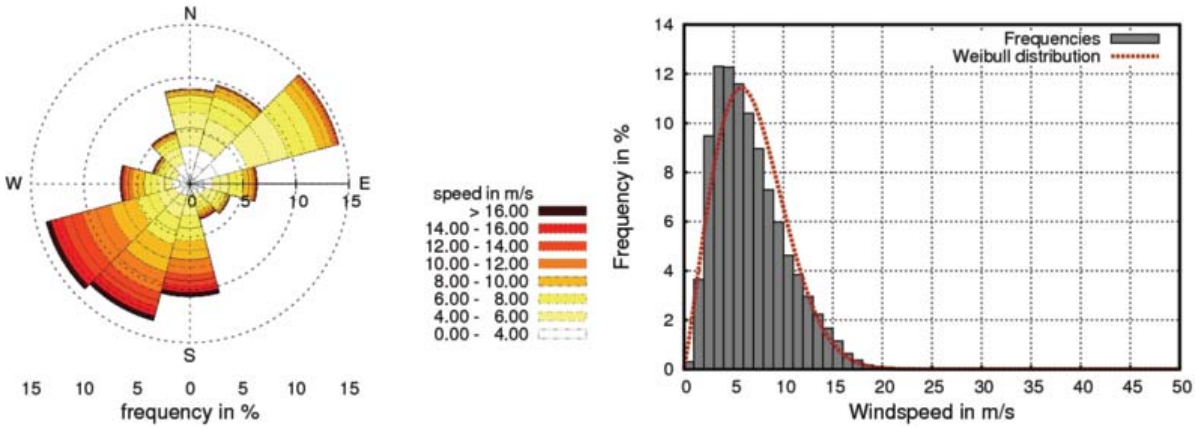

Figure 5.6: Wind rose and Weibull frequency distribution for climatology Local_3

5.2 Setup

5.2.1 Terrain and roughness

The terrain and roughness for the case study is shown in Figure 4.1. Here you can see that most of the elevation at Borg Havn is around 5 m, which makes sense because of the location near the sea. The roughness varies from 0.2 to 0.7 at the port area.

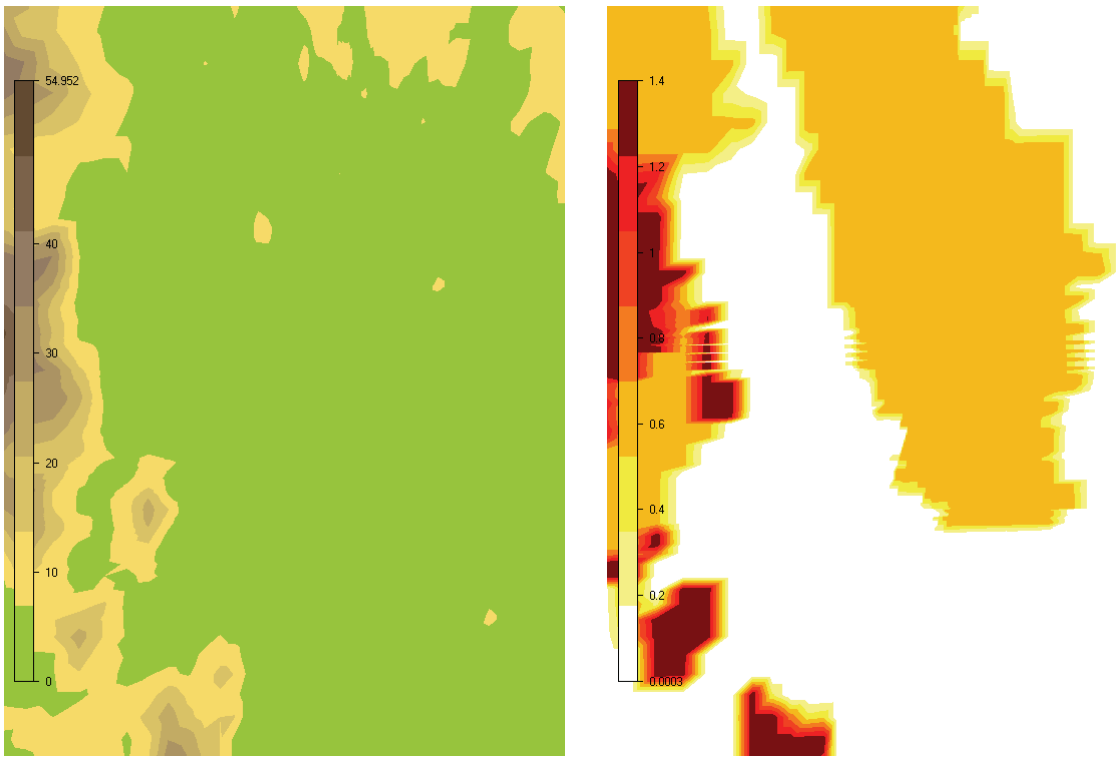

Figure 5.7: Terrain elevation and roughness, legend in meters

5.2.2 BUILDINGS

The buildings were constructed using the blocking file feature in WindSim, described in 3.1.9. The dimensions of the four different buildings are shown in Table 7.

Table 7: Dimensions of buildings constructed at Borg Havn

Building	Length (m)	Width (m)	Height (m)
1	65	45	10
2	21	24	5
3	170	35	14
4	30	30	30

A total of 80 junction points was used to create the four buildings of different sizes. As well as constructing the buildings, the grid had to be sufficient and at the same time practical to build up. Therefore, to make it practical the buildings were orientated at the same angle, facing north-south. This way as a few as possible skew logical lines had to be constructed.

They were built up using the bws-file with global coordinates and edited in a text editor. It was important to not cross each segment as well as making a proper grid to fit the building structures. A distribution factor of 1 were used to make a correct distribution in both i- and j-direction, as well as in k-direction. For the height of the buildings a distribution factor of 1 was chosen to make the grid in z-direction uniform. For the height from the top of the highest building to the boundary layer height a distribution factor of 0.1 was chosen. The resulting grid in all directions of this is shown and described in section 5.2.3. The setup in the bws-file is shown in Table 8.

Table 8: Blocking file used to create the grid and buildings

i-logical :

line_i	points	distribution
1	19	30.0000
2	9	1.0000
3	9	1.0000
4	9	1.0000
5	9	1.0000
6	9	1.0000
7	14	0.0200

j-logical :

line_j	points	distribution
1	19	30.000
2	9	1.0000
3	9	1.0000
4	9	1.0000
5	9	1.0000
6	9	1.0000
7	9	1.0000
8	9	1.0000
9	19	0.0100

k-logical :

line_k	points	distribution	z_upper
1	9	1.0000	5.00
2	9	1.0000	10.0
3	9	1.0000	14.0
4	9	1.0000	30.0
5	9	0.1000	800.0

junctions :

i	j	k	co-ord	x	y
1	1	1	3	610500.00€0	6560354.
2	1	1	3	611803.00€0	6560354.
3	1	1	3	611848.00€0	6560354.
4	1	1	3	611883.00€0	6560354.
5	1	1	3	611904.00€0	6560354.
6	1	1	3	611973.00€0	6560354.
7	1	1	3	612023.00€0	6560354.
8	1	1	3	613000.00€0	6560354.
1	2	1	3	610500.00€0	6561454.
2	2	1	3	611803.00€0	6561454.
3	2	1	3	611848.00€0	6561454.
4	2	1	3	611883.00€0	6561454.
5	2	1	3	611904.0000	6561454.
6	2	1	3	611973.0000	6561454.
7	2	1	3	612023.0000	6561454.
8	2	1	3	613000.0000	6561454.
1	3	1	3	610500.0000	6561484.
2	3	1	3	611803.0000	6561484.
3	3	1	3	611848.0000	6561484.
4	3	1	3	611883.0000	6561484.
5	3	1	3	611904.0000	6561484.
6	3	1	3	611973.0000	6561484.
7	3	1	3	612023.0000	6561484.
8	3	1	3	613000.0000	6561484.
1	4	1	3	610500.0000	6561779.
2	4	1	3	611803.0000	6561779.
3	4	1	3	611848.0000	6561779.
4	4	1	3	611883.0000	6561779.
5	4	1	3	611904.0000	6561779.
6	4	1	3	611973.0000	6561779.
7	4	1	3	612023.0000	6561779.
8	4	1	3	613000.0000	6561779.
1	5	1	3	610500.00€0	6562074.
2	5	1	3	611803.00€0	6562074.
3	5	1	3	611848.00€0	6562074.
4	5	1	3	611883.00€0	6562074.
5	5	1	3	611904.00€0	6562074.
6	5	1	3	611939.00€0	6562074.
7	5	1	3	612107.00€0	6562074.
8	5	1	3	613000.00€0	6562074.
1	6	1	3	610500.00€0	6562109.
2	6	1	3	611803.00€0	6562109.
3	6	1	3	611848.00€0	6562109.
4	6	1	3	611883.00€0	6562109.
5	6	1	3	611904.00€0	6562109.
6	6	1	3	611939.00€0	6562109.
7	6	1	3	612107.00€0	6562109.
8	6	1	3	613000.00€0	6562109.
1	7	1	3	610500.00€0	6562144.
2	7	1	3	611803.00€0	6562144.
3	7	1	3	611848.00€0	6562144.
4	7	1	3	611883.00€0	6562144.
5	7	1	3	611904.00€0	6562144.
6	7	1	3	611939.00€0	6562144.
7	7	1	3	612107.00€0	6562144.
8	7	1	3	613000.00€0	6562144.
1	8	1	3	610500.00€0	6562190.
2	8	1	3	611803.00€0	6562190.
3	8	1	3	611848.00€0	6562190.
4	8	1	3	611883.00€0	6562190.
5	8	1	3	611904.00€0	6562190.
6	8	1	3	611939.00€0	6562190.
7	8	1	3	612107.00€0	6562190.
8	8	1	3	613000.00€0	6562190.
1	9	1	3	610500.00€0	6562209.
2	9	1	3	611803.00€0	6562209.
3	9	1	3	611848.00€0	6562209.
4	9	1	3	611883.00€0	6562214.
5	9	1	3	611904.00€0	6562214.
6	9	1	3	611939.00€0	6562214.
7	9	1	3	612107.00€0	6562214.
8	9	1	3	613000.0000	6562214.
1	10	1	3	610500.0000	6563700.
2	10	1	3	611803.0000	6563700.
3	10	1	3	611848.0000	6563700.
4	10	1	3	611883.0000	6563700.
5	10	1	3	611904.0000	6563700.
6	10	1	3	611939.0000	6563700.
7	10	1	3	612107.0000	6563700.
8	10	1	3	613000.0000	6563700.

junctions_obstacle :

i	j	k	co-ord	x	y

surfaces_obstacle :

i_s	i_e	j_s	j_e	k_s	k_e	type

volumes_obstacle :

i_s	i_e	j_s	j_e	k_s	k_e	kind
4	5	8	9	1	2	obsta
2	3	7	9	1	3	obsta
6	7	5	6	1	4	obsta
6	7	2	3	1	5	obsta

5.2.3 GRID SETUP

The grid was set up by using 85, 110 and 50 cells in x-, y- and z-direction respectively. This makes a total of 467 500 cells. To make the simulations a bit easier to handle and to not affect the grid, the grid consists almost only of straight lines, but some skew to fit the buildings in correctly. In Figure 5.8 the xy-grid is shown on the left, while the grid in z-direction is shown on the right. In Table 9 the distribution and setup for the grid in z-direction is shown.

Table 9: Values in z-direction with corresponding points, distribution and upper values

Line	Points	Distribution	Upper value (m)
1	9	1	5
2	9	1	10
3	9	1	14
4	9	1	30
5	9	0.1	800

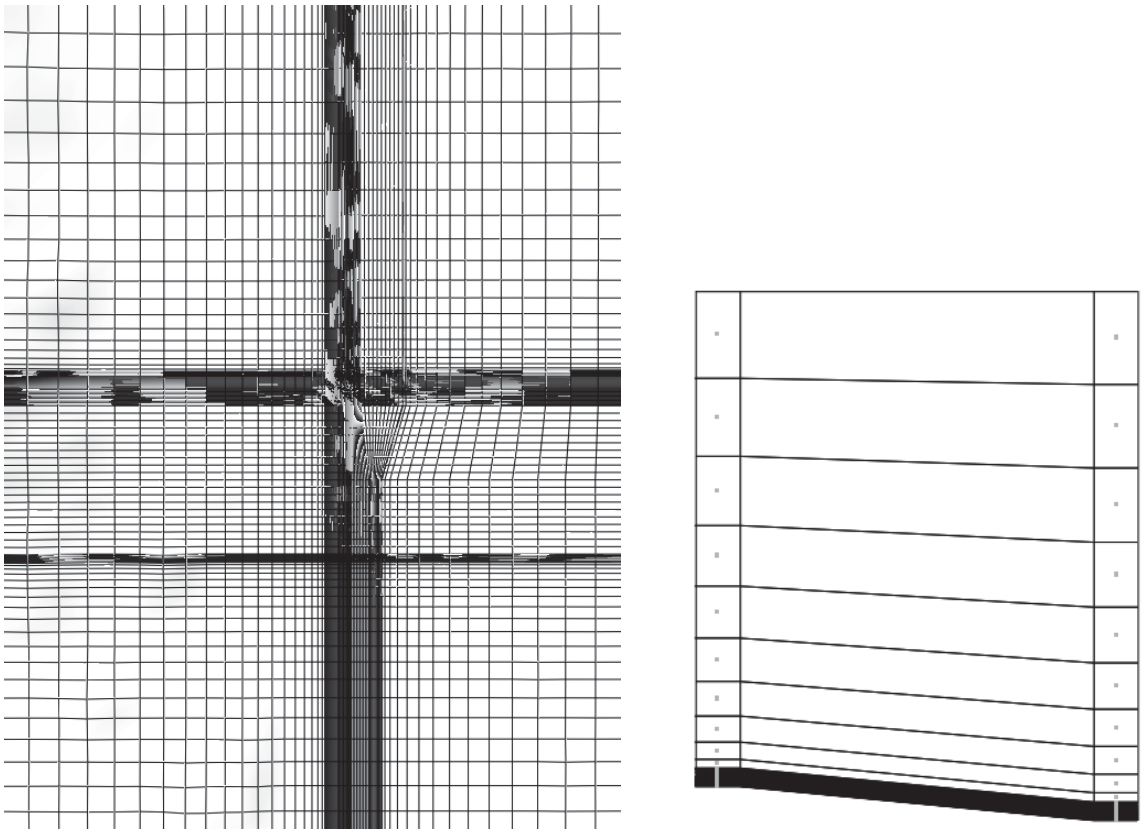

Figure 5.8: Grid in xy- and z-direction

5.2.4 WIND FIELDS

In Table 10 the solver settings for Borg Havn is shown, the same setup was used for both scenarios. The height of the boundary layer was set to 500m and the speed at this height was set to 10m/s, which is default in WindSim. A standard k-ε turbulence model was used. Convergence criteria was set to 0.005. The boundary conditions at top were set to fixed pressure because of the complex terrain.

Table 10: Solver settings

Height of boundary layer (m)	500.0
Speed above boundary layer (m/s)	10.0
Boundary condition at the top	fix pres.
Potential temperature	No
Turbulence model	Standard k-epsilon
Solver	GCV
Maximum iterations	500
Convergence criteria	0.005
Boundary conditions at top	Fixed pressure

For the scenario with buildings you can see from Table 11 that all the sectors except 0, 180, 240 and 270, converges. For the scenario without buildings the same sectors did not converge. The effect from that the sectors that did not converge means a final solution is not obtained and the final results might not be the actual solution. The residual- and spot values are given in Figure 5.9 for sector 0°.

Table 11: Simulation time, number of iterations and convergence status with buildings

Sectors	Simulation time	Iterations	Status	Sectors	Simulation time	Iterations	Status
000	02:08:19	500	-	180	02:11:16	500	-
030	02:00:10	480	C	210	01:47:34	423	C
060	00:59:34	224	C	240	02:05:22	500	-
090	01:17:09	298	C	270	02:06:19	500	-
120	01:01:41	234	C	300	01:54:28	464	C
150	01:41:21	399	C	330	01:24:25	342	C

Table 12: Simulation time, number of iterations and convergence status without buildings

Sectors	Simulation time	Iterations	Status	Sectors	Simulation time	Iterations	Status
000	01:50:49	500	-	180	01:52:11	500	-
030	01:46:27	492	C	210	01:32:21	418	C
060	00:51:55	224	C	240	01:48:60	500	-
090	01:05:57	291	C	270	01:50:27	500	-
120	00:52:55	230	C	300	01:43:52	471	C
150	01:25:12	396	C	330	01:18:27	341	C

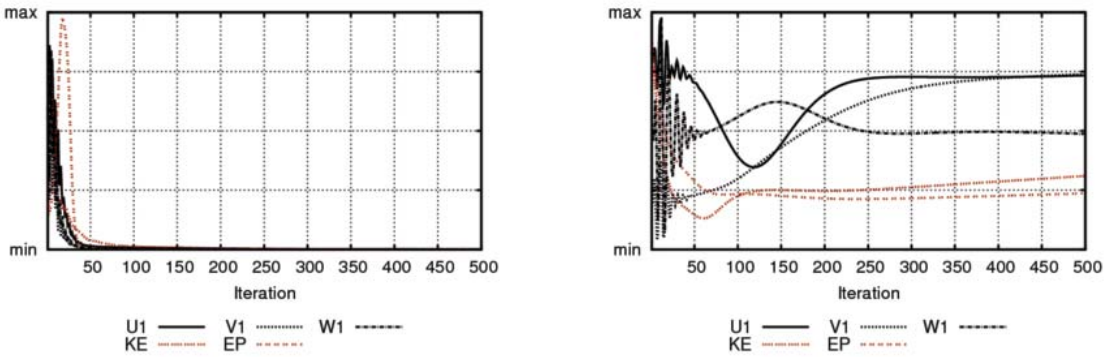

Figure 5.9: Residual values and spot values from convergence study of wind field simulations for sector 0

5.2.1 WIND TURBINE

The chosen wind turbine is a Vestas V39 with a rated power of 500 kW. The hub height was set to 40 m. In Figure 5.10 the power curve for the turbine is shown, while in Table 13 the technical specification is listed.

Table 13: Technical information about the Vestas V39 (Models, 2019).

Turbine type	V39
Rated wind speed (m/s)	15
Cut-in wind speed (m/s)	4
Cut-off wind speed (m/s)	25
Diameter (m)	39.00
air density (kg/m3)	1.225

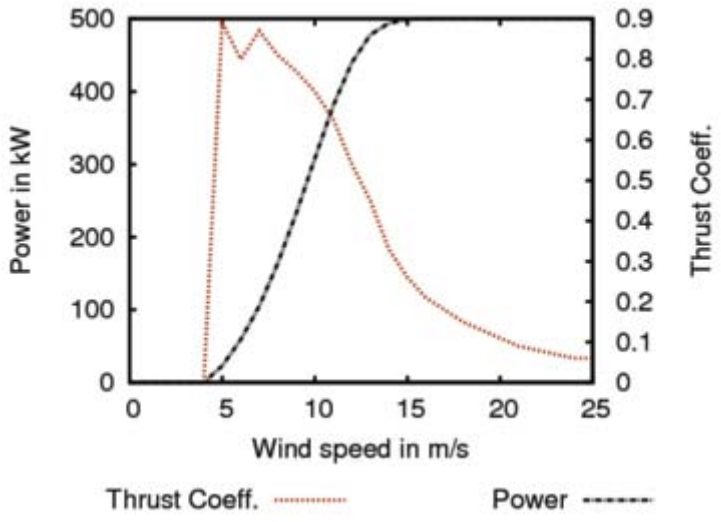

Figure 5.10: Power curve for the Vestas V39 (Vestas, n.d.)

5.2.2 PARK LAYOUT

The park layout for the case study at Borg Havn is shown in 3D in Figure 5.11, as well as from above in Figure 5.12. Here you can see the four different buildings and the placement of the two turbines.

Figure 5.11: Park layout with buildings and turbines

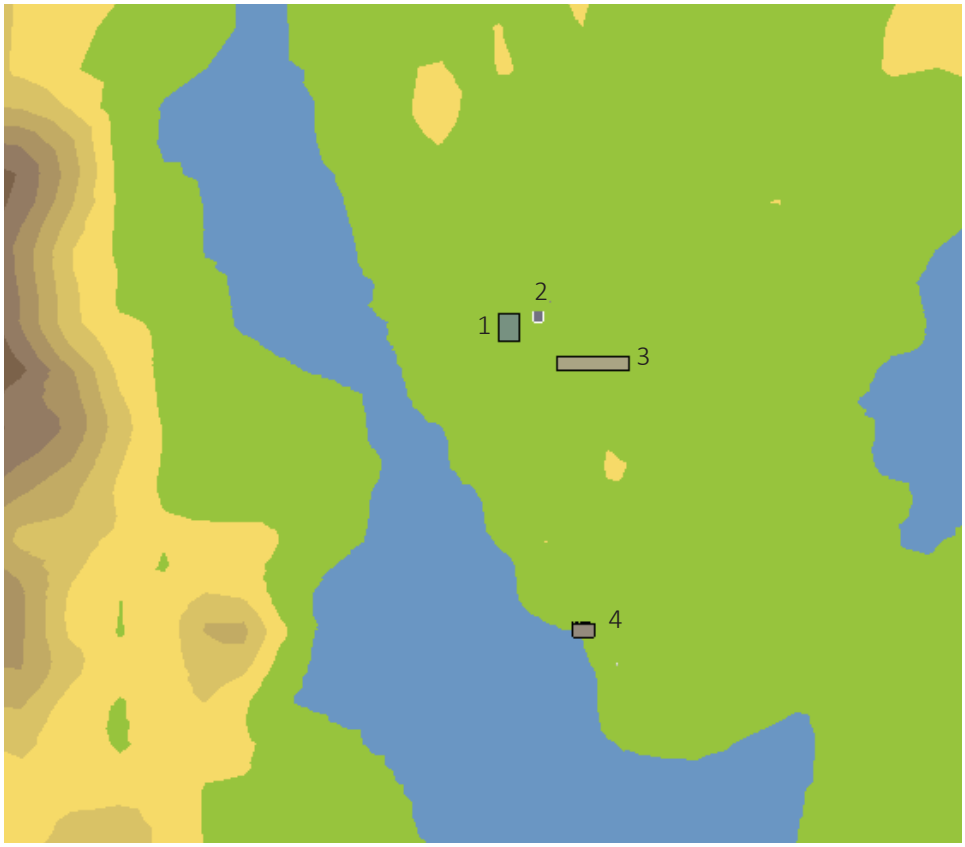

Figure 5.12: Park layout from above

5.3 Results

5.3.1 Wind resources

The wind resources were calculated at heights 6, 10, 20, 30 and 40 meters shown in Figure 5.13 to Figure 5.17 respectively. As you can see from the wind resources at 6m, the buildings create a wake area around them. Most of the wake areas occur from the dominate wind sector 270, hence behind the buildings. At 6m Turbine A is slightly affected while Turbine B is not affected at all. At 10 m height you can see that the wake area is smaller, and that it becomes smaller and smaller for increasing height. At height 30 m only building 4 has a wake area behind and therefore has no effect on the turbines. At 40 m, which is the hub height for the turbines, there is no wake area to be seen, hence there is no reduction of wind speed for the turbines.

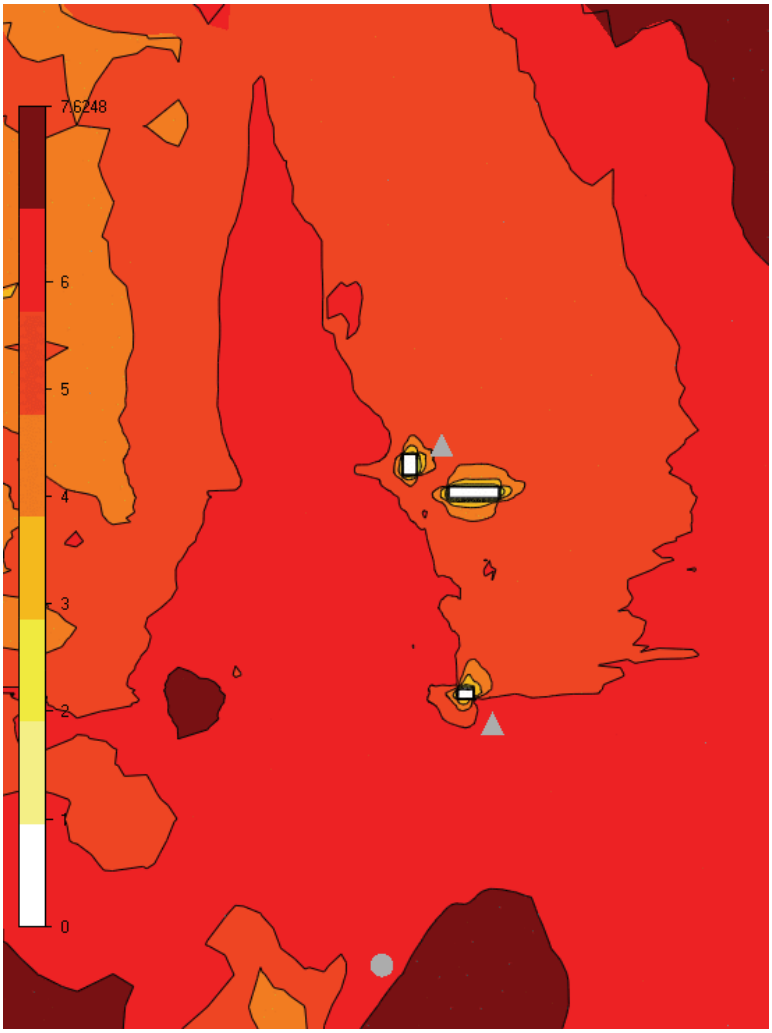

Figure 5.13: Wind resources at 6 m

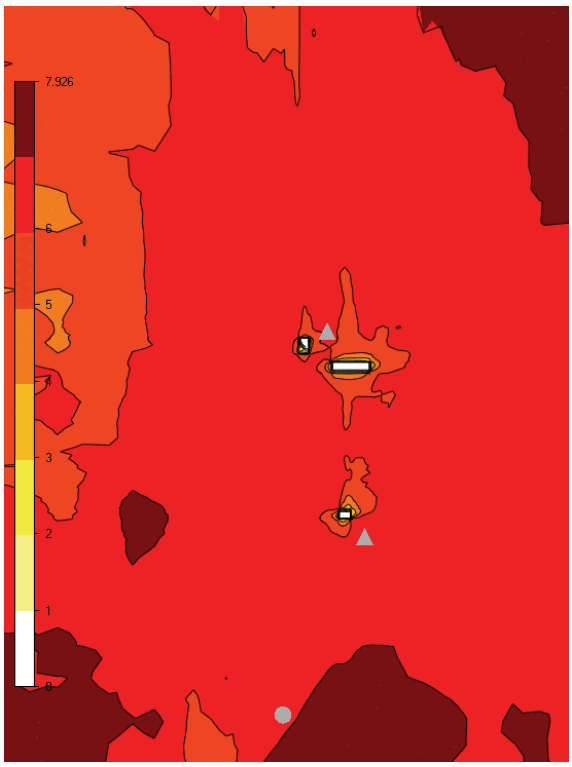

Figure 5.14: Wind resources at 10 m

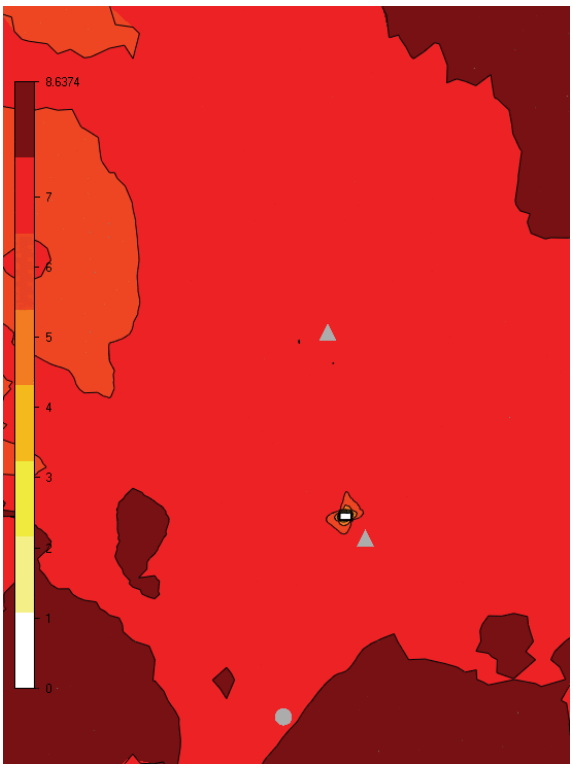

Figure 5.15: Wind resources at 20 m

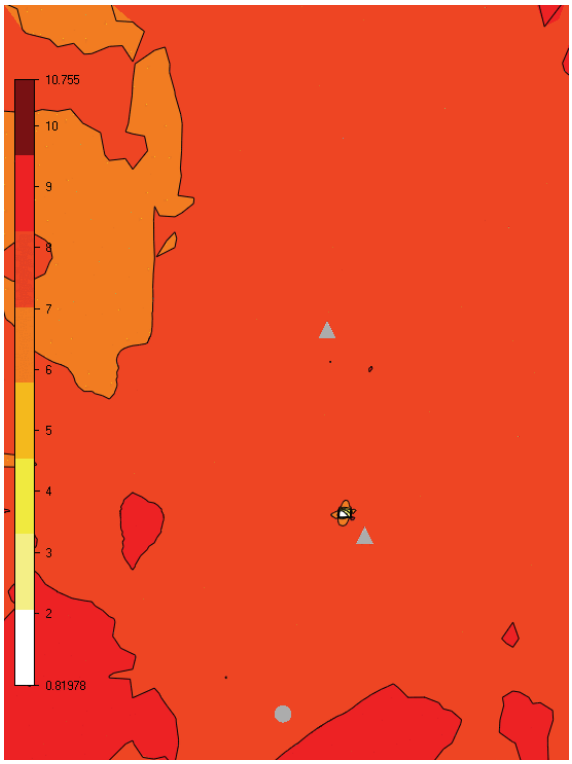

Figure 5.16: Wind resources at 30 m

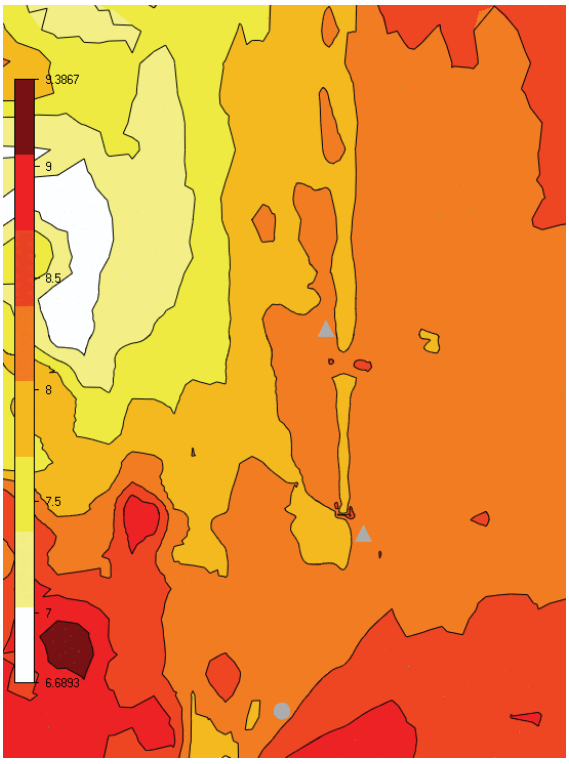

Figure 5.17: Wind resources at hub height 40 m

5.3.2 ANNUAL ENERGY PRODUCTION

The results from the annual energy production (AEP) from the two different scenarios, with and without buildings, in the case study at Borg Havn is given in the following tables. Comparing Table 14 and Table 15 they show that there is no reduction on the AEP in the scenario with buildings. Although, a decrease of 0.01% on the capacity factor is noticeable. The full load hours and average wind speeds remain the same.

Table 14: Total AEP with buildings

Turbine Type	Hub Height (m)	No. of turbines	Capacity (MW)	AEP (GWh/y)	Average wind speed (m/s)	Full load hours (hours)	Capacity factor (%)
V39	40.0	2	1.0	3.3	8.2	3322.7	37.9

Table 15: Total AEP without buildings

Turbine Type	Hub Height (m)	No. of turbines	Capacity (MW)	AEP (GWh/y)	Average wind speed (m/s)	Full load hours (hours)	Capacity factor (%)
V39	40.0	2	1.0	3.3	8.2	3327.3	38.0

Table 16 and Table 17 show the AEP for each of the turbines in the two different scenarios. Here, a more noticeable effect can be seen in difference from the total AEP. At the turbine located in the north of the port, and where there are the most buildings, the results show a reduction of 0.01m/s in average wind speed and an AEP reduction of 0.003 GWh/y. At Turbine B the AEP has a slight reduction, 0.003 GWh/y, but there remains the same wind speed. A reduction of full load hours can also be seen at both turbines.

Table 16: Total AEP per turbine with buildings

Turbine name	Turbine type	Average wind speed (m/s)	AEP (GWh/y)	Full load hours (hours)
Turbine A	V39	8.110	1.647	3294.600
Turbine B	V39	8.270	1.675	3350.800

Table 17: Total AEP per turbine without buildings

Turbine name	Turbine type	Average wind speed (m/s)	AEP (GWh/y)	Full load hours (hours)
Turbine A	V39	8.100	1.650	3299.000
Turbine B	V39	8.270	1.678	3355.600

5.3.3 CUT-PLANES

The cut-planes in xy-plane from Borg Havn show the wake area behind the buildings and how they interfere with the buildings at a height of 6.5m. The cut-plane in Figure 5.18 is extracted from an incidence angle of 270°, which is the dominant wind direction. First, you can see that Turbine B is unaffected by building 4. On the other side, Turbine A is placed in the wake of building 2. Even though this is the smallest building, it still shows some effect. A wind speed reduced from 4 m/s in front, to about 2.5-3 m/s in the wake. Another important observation is that in between buildings 1-3, there is an unaffected area. You can also see from the figure that the wake area extends quite far behind both buildings 1 and 3, and a suction area in front is also indicated. It is important to mention that the cut plane is extracted at 6.5m so this is the affected wake area and not the actual effect on the wind turbines at a height of 40m, which is shown in the wind resource map in Figure 5.17.

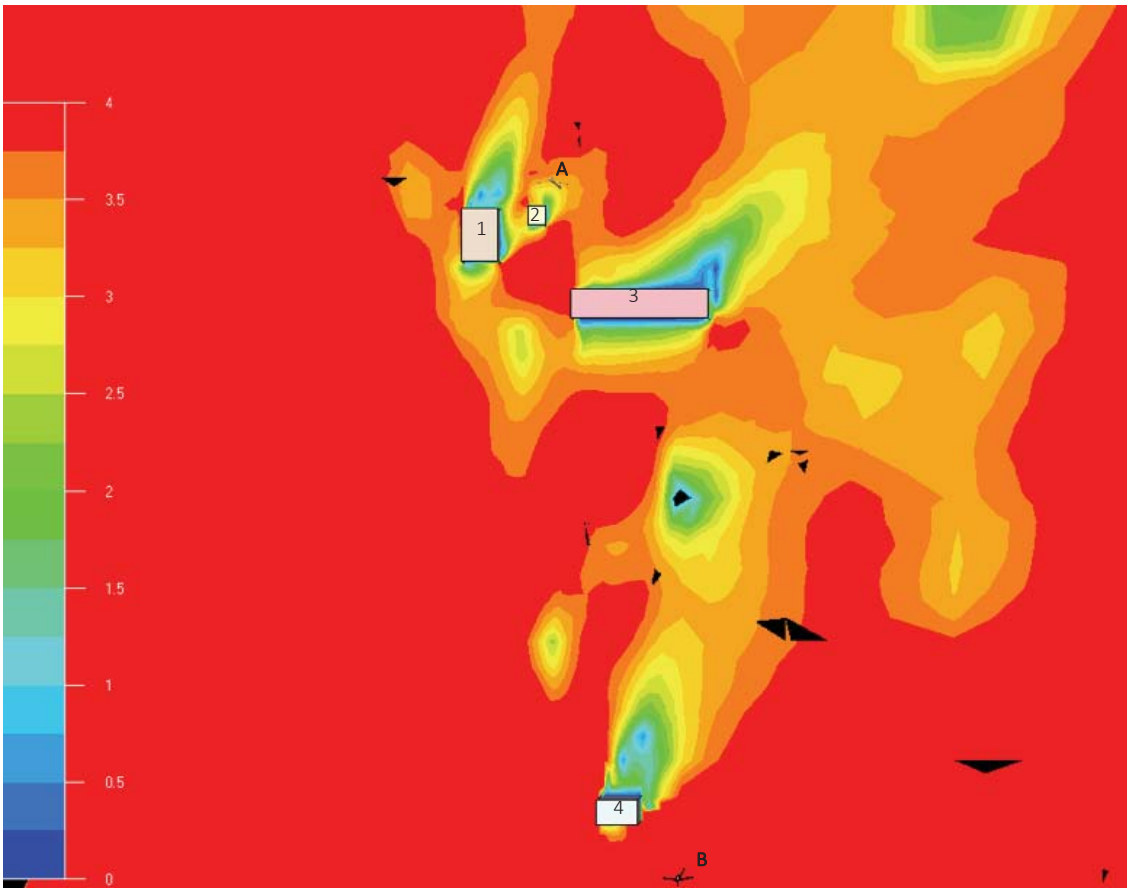

Figure 5.18: Cut-plane in xy-plane from 270° at height 6.5m

In Figure 5.19 a cut-plane in xy-plane with incidence angle 330° is shown, extracted at height 6.5m. Here you can see that from this angle, Turbine A is totally unaffected by the buildings. Another noticeable effect, in difference from Figure 5.18, is that there exists no unaffected area in between buildings 1 to 3. When it comes to Turbine B you can see that the turbine is placed in the wake area. Although there is no significant reduction in wind speed, some effect can be seen.

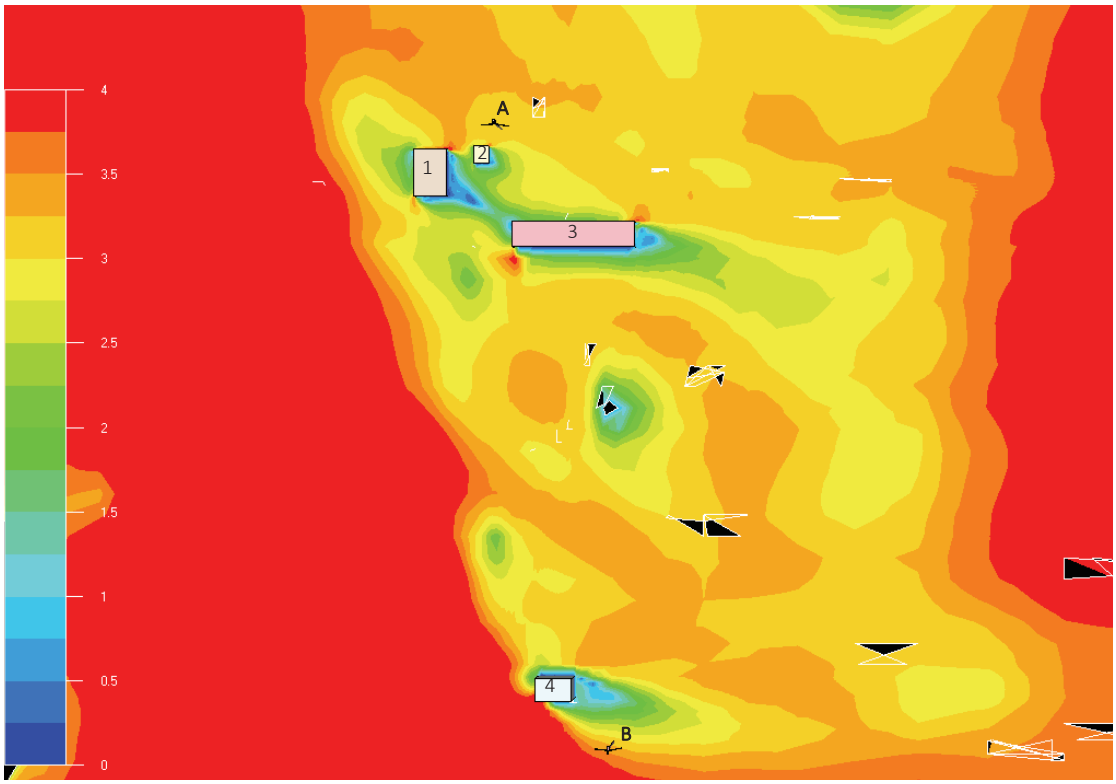

Figure 5.19: Cut-plane in xy-plane from incidence angle 330° at height 6.5m

6 Discussion

6.1 Wind Tunnel Experiment

The study by Castro and Robins (1977) wind tunnel experiment where chosen for the validation of WindSim as a simulation tool for investigating wind flow around buildings. Although Castro and Robins (1977) was an old study it provided the exact necessary information needed for the study, as well as it was frequently used in different studies regarding the same topic which show the quality of the article.

The two different cases, the uniform and logarithmic profile, were chosen as a good comparison basis. The reason why the uniform profile was chosen to be investigated was because this would make a greater foundation for comparison, also, this was not a broadly used aspect in WindSim which led to an interesting study in how the software would comprehend this type of wind profile.

The cut planes constructed needed to be compared even though it is not a sufficient comparison, but gives a good indication of the flow behind an obstacle. Luo et al. (2012) conducted a study in a wind tunnel to investigate the flow, mentioned in 2.5.1. By matching Figure 4.17 and Figure 4.18 with Figure 2.10 you can see that the same wake area is indicated. The reverse flow is both indicated in Figure 2.10 and the results from the experiment. Although Luo et al. (2012) didn't show any results in the front of the obstacle where the suction area evolves, Caniot et al. (2017) study show the same suction area appearing in front. All in all, the cut planes results match well with other studies conducted.

6.2 Methodology

The method used for validation is to be seen as a proper way since the results match well with the reviewed literature. Although some consideration has to be taken in the fact that a real-life scenario compared to numerical simulations do lead to some differences. For the case study the method is also to be seen as sufficient enough to make a basis for the Borg Havn project, since the results show that WindSim is capable of incorporating building structures and obstacles because of the shown wake areas and the reduction in AEP.

The blocking file feature in WindSim was not properly described in literature and took a long time to comprehend and manage properly. It took a great amount of work to master this feature, but the method is to be seen as a suitable function. However, some more information is needed to fully grasp this feature and make full use of it. The opportunity to make buildings with different structures was not investigated in this thesis but could have improved the quality of the simulation done.

6.3 WindSim vs Wind tunnel

The vertical profiles presented in the results section indicate the capability of WindSim. The different figures show almost the exact same measurements as done by Castro and Robins (1977), although with some deviation. The most important differences to mention is the negative wind speed measured by Castro and Robins (1977) which WindSim could not generate. But the figures show the same skew graph at the same height, although with reduced and not negative wind speeds. Also shown in the figures for -1H, in front of the obstacle, and 1H, directly behind the obstacle, a skew graph occurs. This corresponds well with the cut planes and Castro and Robins (1977) measurements. This is revealed with the decreasing wind speed at these distances. You can also see that for Case A, at a distance of 2H, there is some recirculation, but for Case B there is no indication of recirculation.

The recirculation is shown in the cut planes and vector fields. They match the vertical wind profiles as well as matching the literature regarding this occurrence. For the comparison of Case A and B, the recirculation area and eddies show differences bot in the vertical and horizontal perspectives. The reattachment distance and zone are clearly different, as you can perceive in Case A, the reattachment zone is outside of the wind tunnel, which is also indicated in Figure 4.31. In the case of the logarithmic profile the reattachment clearly occurs at a distance of 9.5H

downstream, and at 5H the reattachment is almost at the same as the inlet. This matches well with what was found by Castro and Robins (1977), that at 4.5H the reattachment was almost obtained and at 8.5H the reattachment was complete.

The figure from Nieuwpoort et al. (2010) shown in Figure 2.5, indicates that it develops a skew wind profile directly behind the obstacle at around 1H, as well as a smaller one further behind. This corresponds well with Figure 4.26 which also shows this type of wind profile at 1H. Further behind, at around 3-4H, in Nieuwpoort et al. (2010) figure, the wind profile almost reattaches. This again, resembles well with the results in Figure 4.30.

Figure 2.7 from Wegley et al. (1980) shows the area of disturbed flow. Although the measurements which Wegley et al. (1980) proposes, a distance of 20H behind the obstacle and 2H in height, don't match the results. Although the estimate of 2H fits well with the vertical profile, and the disturbed flow area also is pretty similar which both is shown in the vertical profile in Figure 4.18.

6.4 Borg Havn

To complement the validation of WindSim as a satisfactory tool, the case study at Borg Havn were done. This was to transfer the knowledge from the literature and validation to a real-life scenario. This was done to mainly look at the cut planes, wind resources and AEP, and not to actually, do a resources assessment since real measurements from Borg Havn was not obtained.

Firstly, the wind resource map gives a good indication on how the wake area develops from all of the sectors at Borg Havn. You could see from Figure 5.13 to Figure 5.17 that the wake area gets smaller the higher above ground it gets. At hub height 40m the map shows that there is no affected area for the wind turbines, although at 6m it shows that the wake area could affect the turbines. The cut planes also give a good indication of the wake area behind the buildings. Figure 5.18 and Figure 5.19 gives a clear view of the suction, reattachment and wake area. The cut planes match the wind resource map well but shows the developing wake area better from the dominant wind direction. The figures also corresponds well with what Caniot et al. (2017) found using UrbaWind. The wake area behind the buildings also matches the cut planes from the wind tunnel experiment, although in the figures for Borg Havn have different incidence angle, they show almost the same evolving wake profile.

The results were not as expected in the sense of the minor differences in the two scenarios, with and without buildings. Without the buildings, the AEP for Turbine A located near the three buildings on the north side of the port was at 1.650 GWh/y. This compared to the scenario with buildings had a reduction of 3000 kWh/y. Although this is a small reduction, it indicates that the buildings have some effect. For Turbine B located near the tallest building a reduction of 3000 kWh/y also occurred, indicating the same effect. Since the dominating wind direction was from south-west in the climatology, this is a bit strange due to the location of the building on the west side of the turbine.

Another important aspect is that the buildings located near Turbine A ranged from 5-15m and the hub height was 40m. Turbine B located near the building which had a height of 30m you would expect a larger effect, but due to mentioned wind direction this might lead to the same AEP reduction. Another explanation to the low effect can be that no variations were detected because of a too coarse grid in z-direction, or too coarse resolution at the turbine positions.

6.5 Limitations

One of the limitations in this study is the comparison of a real wind tunnel and a numerical study. Although the comparison shows a good match, the fact that WindSim is a numerical software leads to some differences in the setup.

In the case of Castro and Robins (1977) they also conducted an experimental setup of a incidence angle of 45 ° which also could be used as a validation foundation, also comparing with Caniot et al. (2017) work. Due to the minor differences, and the fact that WindSim corresponded that well for an incidence angle of 0°, the validation that was done were seen to be sufficient. There are also some consideration to be taken in the data from Castro and Robins (1977) which was extracted manually from figures, hence, some minor differences could occur from this.

Another limitation is the grid resolution regarding the number of cells in both the validation and case study. A higher number of cells could have been used, but due to limited computational power the chosen number of cells were concluded to be sufficient for this thesis. Also, there has not been utilized a grid independency test, this could have resulted in a better resolution on the simulations.

The dimensions were also picked up from Google Earth which might lead to some uncertainties on the actual heights of the building. Further on, at Borg Havn, the buildings were set to have a straight angle facing north-south in 180°. This was to make the grid easier to set up and to make the grid well dimensioned. Other incidence angles would do the gridding more difficult and maybe weaker. The buildings that were constructed of course were not orientated in this matter in real life, but the significance of this were to be seen as rather small. The simulations done at Borg Havn were also only done with flat roofs. It's obvious that is not valid for all the buildings so a further study in this could be done. By utilizing Ntinas et al. (2014) a validation of the WindSim software capability to comprehend it and further make use of this in the simulation.

7 Conclusion

The objective of this thesis was to explore urban wind and its challenges regarding how building affects the annual energy production from the wind turbine. The purpose was to use already established knowledge and to further investigate this with WindSim. The significance of this work is to be seen as a great amount because of the fact that urban wind studies have almost only consisted of roof mounted turbines, and not commercial scale turbines. This combined with the fact that obstacle effects on the wind flow has been thoroughly studied, but further study to transfer this to buildings and the effect on commercial scale turbines had not been done in a broader perspective.

The main findings show that WindSim is a suitable tool to investigate the effect of buildings on energy production. The blocking file feature clearly make a good tool to investigate such challenges as this thesis focused on. Also, the fact that the buildings at Borg Havn had a small effect on the annual energy production show that the buildings have some effect, although not remarkable. This again show that WindSim and numerical simulations have great potential to help study this further and to be used in further work.

7.1 Further work

For further work the validation case could be done with different incidence angles, as well as for the buildings in the case study. This in combination with looking at different roof geometries could have led to a more thoroughly study. The effect of building canyons could also have been studied to see if there were any positive effect of buildings. The grid resolution could have been increased, and the wind field simulation could result in different results after reaching grid independency, in this thesis. This have a greatly impact on the wind flow around the buildings and is an important aspect to investigate regarding urban wind energy.

8 References

Alfonsi, G. (2009). *Reynolds-Averaged Navier-Stokes Equations for Turbulence Modeling*, vol. 62.

Beller, C. (2009). *Urban Wind Energy - State of the Art*. Report. www.dtu.dk: Techinical University of Denmark.

Bravard, J. P. & Petit, F. (2009). Geomorphology of Streams and Rivers. In Likens, G. E. (ed.) *Encyclopedia of Inland Waters*, pp. 387-395. Oxford: Academic Press.

Caniot, G., Li, W. & Dupont, G. (2017). *Validations and applications of a CFD tool dedicated to wind assessment in urban areas*.

Castro, I. P. & Robins, A. G. (1977). The flow around a surface-mounted cube in uniform and turbulent streams. *Journal of Fluid Mechanics*, 79 (2): 307-335. doi: 10.1017/S0022112077000172.

Chiu, J.-J. & Chien, S. (2011). Effects of Disturbed Flow on Vascular Endothelium: Pathophysiological Basis and Clinical Perspectives. *Physiological Reviews*, 91 (1): 327-387. doi: 10.1152/physrev.00047.2009.

Danish Wind Industry Association. (2003). *Roughness and Wind Shear*: Danish Wind Industry Association. Available at: http://xn--drmstrre-64ad.dk/wp-content/wind/miller/windpower%20web/en/tour/wres/shear.htm (accessed: 29 April 2019).

EIA. (2018). *Wind Explained: History of Wind Power*. Web Article: The U.S. Energy Information Administration (EIA). Available at: https://www.eia.gov/energyexplained/index.php?page=wind_history (accessed: 26.02).

Emeis, S. & Turk, M. (2007). Comparison of Logarithmic Wind Profiles and Power Law Wind Profiles and their Applicability for Offshore Wind Profiles. In, pp. 61-64.

Holmes, J. D. (2018). *Wind loading of structures*: CRC press.

Integrated Publishing. (n.d.). *AEROGRAPHER'S MATE, MODULE 05--BASIC METEOROLOGY*. tpub.com: Integrated Publishing. Available at: http://meteorologytraining.tpub.com/14312/css/14312_82.htm (accessed: 8 May 2019).

Kida, S. (2001). Life, Structure, and Dynamical Role of Vortical Motion in Turbulence. *IUTAMim Symposium on Tubes, Sheets and Singularities in Fluid Dynamics*.

Li, D. (2018). *Wind resource assessment for Borg Havn*, 180227_BorgHavn_100: WindSim AS.

Luo, W., Dong, Z., Qian, G. & Lu, J. (2012). Wind tunnel simulation of the three-dimensional airflow patterns behind cuboid obstacles at different angles of wind incidence, and their significance for the formation of sand shadows. *Geomorphology*, 139-140: 258-270. doi: https://doi.org/10.1016/j.geomorph.2011.10.027.

Majda, A. J. & Bertozzi, A. L. (2002). *Vorticity and incompressible flow*, vol. 27: Cambridge university press.

Manwell, J., McGowan, J. & L Rogers, A. (2009). Wind Energy Explained: Theory, Design and Application, Second Edition. In vol. 30.

Meroney, R. (1985). *Wind flow patterns about buildings*, vol. 21.

Models, W. T. (2019). *Vestas V39*. wind-turbine-models.cm: Wind turbine models. Available at: https://en.wind-turbine-models.com/turbines/383-vestas-v39#powercurve.

Nieuwpoort, A. M. H., Gooden, J. H. M. & Prins, J. L. d. (2010). *Wind criteria due to obstacles at and around airports*. https://skybrary.aero/bookshelf/books/2281.pdf: National Aerospace Laboratory NLR ; DGTL.

Ntinas, G. K., Zhang, G., Fragos, V. P., Bochtis, D. D. & Nikita-Martzopoulou, C. (2014). Airflow patterns around obstacles with arched and pitched roofs: Wind tunnel

measurements and direct simulation. *European Journal of Mechanics - B/Fluids*, 43: 216-229. doi: https://doi.org/10.1016/j.euromechflu.2013.09.004.
Oke, T. R. (2002). *Boundary layer climates*: Routledge.
Piff, M. (1991). *Discrete mathematics: an introduction for software engineers*: Cambridge University Press.
Schoch, R. B., Han, J. & Renaud, P. (2008). Transport phenomena in nanofluidics. *Reviews of modern physics*, 80 (3): 839.
Troen, I. & Petersen, E. L. (1989). *European Wind Atlas*: Risø National Laboratory, Roskilde.
Versteeg, H. K. & Malalasekera, W. (2007). *An introduction to computational fluid dynamics: the finite volume method*: Pearson education.
Vestas. (n.d.). *Vestas V39*.
Wegley, H. L., Ramsdell, J. V., Orgill, M. M. & Drake, R. L. (1980). *Siting handbook for small wind energy conversion systems*: Battellle Pacific Northwest Lab.
Wieringa, J. (1998). How farn can agrometerological station observations be considered representative? *Preprint to 23rd Amer. Meteor. Soc. Conference on Agric. and Forest Meteor*.
Wikipedia contributors. (2019). *K-epsilon turbulence model*. 876449280 ed.: Wikipedia, The Free Encyclopedia. Available at: https://en.wikipedia.org/w/index.php?title=K-epsilon_turbulence_model&oldid=876449280 (accessed: 5 May 2019).
WindSim. (2019). *WindSim - Technical Basics*: WindSim. Available at: https://windsim.com/software/windsim---technical-basics.aspx.

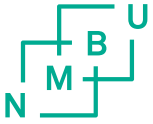

Norges miljø- og biovitenskapelige universitet
Noregs miljø- og biovitskapelege universitet
Norwegian University of Life Sciences

Postboks 5003
NO-1432 Ås
Norway